NASA TECHNICAL NOTE

NASA TN D-6993

NASA TN D-6993

SUMMARY OF DIRECTIONAL DIVERGENCE CHARACTERISTICS OF SEVERAL HIGH-PERFORMANCE AIRCRAFT CONFIGURATIONS

by H. Douglas Greer

Langley Research Center
Hampton, Va. 23365

NATIONAL AERONAUTICS AND SPACE ADMINISTRATION • WASHINGTON, D. C. • NOVEMBER 1972

1. Report No.	2. Government Accession No.	3. Recipient's Catalog No.
NASA TN D-6993		

4. Title and Subtitle	5. Report Date
SUMMARY OF DIRECTIONAL DIVERGENCE CHARACTERISTICS OF SEVERAL HIGH-PERFORMANCE AIRCRAFT CONFIGURATIONS	November 1972
	6. Performing Organization Code
7. Author(s)	8. Performing Organization Report No.
H. Douglas Greer	L-8489
	10. Work Unit No.
9. Performing Organization Name and Address	501-26-04-02
NASA Langley Research Center Hampton, Va. 23365	11. Contract or Grant No.
	13. Type of Report and Period Covered
12. Sponsoring Agency Name and Address	Technical Note
National Aeronautics and Space Administration Washington, D.C. 20546	14. Sponsoring Agency Code

15. Supplementary Notes

16. Abstract

The present paper summarizes the high-angle-of-attack characteristics of a number of high-performance aircraft as determined from model force tests and free-flight model tests and correlates these characteristics with the dynamic directional-stability parameter $C_{n_{\beta,dyn}}$. This correlation shows that $C_{n_{\beta,dyn}}$ correlates fairly well with directional divergence. Data are also presented to show the effect of some airframe modifications on the directional divergence potential of the configuration. These results show that leading-edge slats seem to be the most effective airframe modification for reducing or eliminating the directional divergence potential of aircraft with moderately swept wings.

17. Key Words (Suggested by Author(s))

Directional divergence
Lateral stability
Directional divergence parameter

18. Distribution Statement

Unclassified – Unlimited

19. Security Classif. (of this report)	20. Security Classif. (of this page)	21. No. of Pages	22. Price*
Unclassified	Unclassified	62	$3.00

*For sale by the National Technical Information Service, Springfield, Virginia 22151

SUMMARY OF DIRECTIONAL DIVERGENCE CHARACTERISTICS OF SEVERAL HIGH-PERFORMANCE AIRCRAFT CONFIGURATIONS

By H. Douglas Greer
Langley Research Center

SUMMARY

Many high-performance jet airplanes have exhibited a directional divergence at angles of attack near the stall. The divergence is usually associated with aircraft having highly swept wings and can lead to large losses in altitude and spins, which can result in losses of airplanes and aircrews. A considerable amount of information has been generated by past investigations of specific airplane configurations. The present paper summarizes much of this information with special regard to the correlation of experimental data with a dynamic directional-stability parameter known as $C_{n_{\beta,dyn}}$. Much experimental data come from free-flight dynamic model tests and wind-tunnel force tests of these same models. A limited amount of full-scale flight data is available for correlation with the model tests.

This summary shows that many, if not most, high-performance airplane configurations exhibit the directional divergence at high angles of attack. The divergence can be predicted in most cases by the criterion that when $C_{n_{\beta,dyn}}$ is negative, a divergence will be experienced. Leading-edge slats are found to be the most effective device for eliminating the directional divergence or delaying it to higher angles of attack, at least for airplanes with wings of moderate sweep.

INTRODUCTION

Many high-performance jet aircraft have exhibited a directional divergence when flown at angles of attack near or above the stall. The directional divergence is usually associated with aircraft having highly swept or delta wings. Conditions for divergence can occur during landing approach, take-off, or in maneuvers, especially during combat maneuvers where the pilot may inadvertently cause the aircraft to reach very high angles of attack. The divergence can lead to a spin from which a recovery might or might not be obtained, or if the divergence occurs at low altitude, the likely result would be the loss of the aircraft and probably the crew.

Experience has shown that the divergence does not correlate with simple static directional stability as measured in a wind tunnel, but is a more complicated dynamic

phenomenon. A dynamic directional-stability parameter called $C_{n_{\beta,dyn}}$, which can be determined from wind-tunnel force tests, was developed many years ago to serve as a criterion for prediction of the possibility of a directional divergence and correlates fairly well with the directional divergence characteristics shown by free-flight model tests. Considerable experience has been gained in this problem area over the past 20 years, but the results of this experience have never been summarized. The purpose of the present paper is to summarize the experience of the NASA Langley Research Center, most of it with free-flight models and wind-tunnel force tests of these same models at the same value of Reynolds number. This combination of model test techniques offers an exceptional opportunity for correlation of wind-tunnel and flight because it eliminates the two principal factors which often thwart such correlation – differences in Reynolds number and configuration.

The present paper summarizes the high-angle-of-attack characteristics of a number of high-performance aircraft as determined from model force tests and free-flight tests and correlates these characteristics with the dynamic directional-stability parameter $C_{n_{\beta,dyn}}$. Data are also presented to show how several airframe modifications affect the static lateral-stability parameters $(C_{n_\beta}$ and $C_{l_\beta})$ and $C_{n_{\beta,dyn}}$, and thereby offer means for altering the divergence potential of a configuration. The derivation of $C_{n_{\beta,dyn}}$ from the lateral equations of motion is given in the appendix.

SYMBOLS

All aerodynamic data with the exception of lift are presented with respect to a body system of axes. The lift data are presented with respect to the wind axes (fig. 1). Dimensional values herein are given in the International System of Units (SI) (ref. 1).

A,B,C,D,E	coefficients of lateral-stability quartic
b	wing span, m
C_L	lift coefficient, $\frac{\text{Lift}}{qS}$
C_l	rolling-moment coefficient, $\frac{\text{Rolling moment}}{qSb}$
C_n	yawing-moment coefficient, $\frac{\text{Yawing moment}}{qSb}$
$C_{n_{\beta,dyn}}$	directional divergence parameter, $C_{n_\beta} - \frac{I_Z}{I_X} C_{l_\beta} \sin \alpha$

$C_R = \frac{C}{K}$

$C_R' = C_{n_\beta} \cos \alpha - \frac{I_Z}{I_X} C_{l_\beta} \sin \alpha$

C_Y side-force coefficient, $\frac{\text{Side force}}{qS}$

F_D drag force, N

F_L lift force, N

F_Y side force, N

I_X moment of inertia about longitudinal body axis, kg-m^2

I_Z moment of inertia about normal body axis, kg-m^2

$K = \frac{4mI_X}{\rho^2 S^2 b^4}$

K_{X_o} nondimensional radius of gyration in roll about principal longitudinal axis, $\frac{I_X}{mb^2}$

K_{Z_o} nondimensional radius of gyration in yaw about principal normal axis, $\frac{I_Z}{mb^2}$

M_X rolling moment, m-N

M_Y pitching moment, m-N

M_Z yawing moment, m-N

m aircraft mass, kg

p rolling velocity, rad/sec

q free-stream dynamic pressure, N/m^2

r	yawing velocity, rad/sec
S	wing area, m^2
V	velocity, m/sec
X,Y,Z	longitudinal, lateral, and normal axes, respectively (fig. 1)
α	angle of attack, deg
β	angle of sideslip, deg
δ_e	elevator deflection (positive when trailing edge down), deg
Λ	leading-edge sweep, deg
λ	root of lateral-stability quartic
μ_b	lateral-directional relative-density factor, $m/\rho Sb$
ρ	mass density of air, kg/m^3

$$C_{l_\beta} = \frac{\partial C_l}{\partial \beta} \qquad C_{n_\beta} = \frac{\partial C_n}{\partial \beta} \qquad C_{Y_\beta} = \frac{\partial C_Y}{\partial \beta}$$

$$C_{l_p} = \frac{\partial C_l}{\partial \frac{pb}{2V}} \qquad C_{n_p} = \frac{\partial C_n}{\partial \frac{pb}{2V}} \qquad C_{Y_p} = \frac{\partial C_Y}{\partial \frac{pb}{2V}}$$

$$C_{l_r} = \frac{\partial C_l}{\partial \frac{rb}{2V}} \qquad C_{n_r} = \frac{\partial C_n}{\partial \frac{rb}{2V}} \qquad C_{Y_r} = \frac{\partial C_Y}{\partial \frac{rb}{2V}}$$

PRESENTATION OF DATA

Presented in figure 1 are sketches defining the axis systems and positive directions of the force and moment data are indicated.

Figure 2 presents time histories of flight data obtained from the flight recorder of a full-scale test aircraft during a directional divergence.

Data from 17 different aircraft configurations are presented. These configurations (designated A to Q) have been categorized as fighters, bombers, and transports. Included in the fighter group are research aircraft of fighter size and configuration. Plan views of the configurations are presented as follows: Fighters in figure 3; bombers in figure 4; and transports in figure 5.

Presented in figures 6 to 22 are wind-tunnel static-force test data for the configurations discussed in this paper. The force test data are presented with zero control deflection unless otherwise specified. Note that for figures 13(b), 17(b), and 19(b) the scale for $C_{n_{\beta,dyn}}$ has been changed for convenience of plotting.

BACKGROUND ON $C_{n_{\beta,dyn}}$ AS A CRITERION

In the late 1940's low-aspect-ratio swept-wing fighter configurations began to emerge, and it soon became apparent that they could behave very differently at the stall from their predecessor straight-wing configurations. Whereas straight-wing configurations generally experienced a roll-off type of divergence at the stall because of one wing stalling before the other and unstable damping in roll immediately beyond the stall, the swept-wing configurations began to show a directional divergence at high angles of attack.

In order to illustrate a directional divergence, a time history of an actual flight test of configuration J is presented in figure 2 (ref. 2). The traces presented in this figure show the major flight variables and control-surface deflections as a function of time. During the time period represented on these traces, the pilot was attempting to make a 60° banked turn to the left. After the pilot rolled into the turn, the angle of attack was increased at a fairly constant rate. At approximately 38 seconds, the normal acceleration began to decrease even though the angle of attack was still increasing, thereby indicating major stall. At approximately 50 seconds the aircraft diverged violently and entered a $2\frac{1}{2}$-turn spin to the right. This example shows not only what occurs during a divergence, but with the aircraft entering a spin, clearly illustrates the seriousness of the divergence problem.

Langley's first experience with directional divergence was encountered during tests of dynamically scaled flying models of configurations B (ref. 3) and C (ref. 4) in the Langley free-flight tunnel. From tests of these two configurations together with configuration A (ref. 5), it was apparent that the problem was more complicated than one of simple static directional instability $\left(\text{negative } C_{n_\beta}\right)$. Configurations A and B, which had similar geometric characteristics, both had negative values of C_{n_β} at high angles of attack; but configuration B diverged, whereas configuration A did not. One aerodynamic difference was that configuration A had positive dihedral effect $\left(-C_{l_\beta}\right)$ at high angles of attack, whereas configuration B had negative dihedral effect $\left(+C_{l_\beta}\right)$. Similarly, configura-

tion C diverged in the clean condition, whereas it did not diverge with slats extended, although both conditions had negative directional stability at high angles of attack. Here again the model diverged when C_{l_β} was positive and not when C_{l_β} was negative. The experimenting aerodynamicist quickly related these facts that a combination of $-C_{n_\beta}$ and $+C_{l_\beta}$ resulted in a directional divergence but that a combination of $-C_{n_\beta}$ and $-C_{l_\beta}$ did not. Then the dynamicist became aware of the problem and suggested that the moment of inertia differences of the old and new fighter configurations might be a contributing factor. A theoretical analysis group headed by Leonard Sternfield, then of Langley, studied the problem and concluded that the divergences occurred when the C-term of the stability quartic became negative and they developed a simplified form of the C-term and called it $C_{n_{\beta,dyn}}$, or the dynamic directional-stability parameter. The derivation of this parameter is given in the appendix.

The term $C_{n_{\beta,dyn}}$ seemed to correlate reasonably well with the directional divergence characteristics observed with configurations A, B, and C, and subsequent dynamic models; but at that time there were some unexplained exceptions. Because of the beginning of the air-launched missile era when fighters were not going to be maneuvered to high angles of attack, no summation of the experience with directional divergence and the correlation with $C_{n_{\beta,dyn}}$ was ever made, even though most of the experience was gained 10 to 15 years ago.

CORRELATION OF $C_{n_{\beta,dyn}}$ WITH DIRECTIONAL DIVERGENCE

A summary of the divergence characteristics of the configurations discussed in this paper is presented in table I along with an indication as to how well the directional divergence parameter correlated with the actual divergence characteristics. The correlations are rated as good, fair, and poor. The rating of good was assigned to configurations for which $C_{n_{\beta,dyn}}$ correctly indicated no divergence or correctly indicated a divergence and the angle of attack at which it occurred. Table I shows that the correlation was good in nearly two-thirds of the cases shown. This shows that $C_{n_{\beta,dyn}}$ can be a useful tool in predicting the occurrence of directional divergence; and, since the aerodynamic terms in the expression $C_{n_{\beta,dyn}}$ can be measured during static-force tests, it is relatively easy to get an indication of whether or not the airplane might experience a directional divergence. However, to determine the maximum usefulness of $C_{n_{\beta,dyn}}$, the cases with fair or poor correlation must be examined to study the limitations of the parameter $C_{n_{\beta,dyn}}$ in predicting directional divergence. The fair and poor ratings are used to designate configurations for which $C_{n_{\beta,dyn}}$ either fails to predict accurately the angle of attack at which a divergence occurs or fails to predict a divergence altogether.

The ability of $C_{n_{\beta,dyn}}$ to predict directional divergence accurately can be affected in several ways.

For example, included in the fair rating are configurations J and N (ref. 6 and unpublished data) for which $C_{n_{\beta,dyn}}$ did not become negative but for which there was a dip in the curve for $C_{n_{\beta,dyn}}$ which approached zero at the angle where the divergence occurred. It is possible in these cases that the data points plotted to obtain the curves presented do not represent the extremes of the curves and that negative values of $C_{n_{\beta,dyn}}$ exist between two of the points that were plotted. Another possibility deals with the terms that were neglected in reducing the C-coefficient of the lateral equation of motion to $C_{n_{\beta,dyn}}$. It is possible that for these configurations the values of these terms are large enough to cause the C-coefficient (for which $C_{n_{\beta,dyn}}$ is an approximation) to become negative at points where $C_{n_{\beta,dyn}}$ approaches zero.

Another factor which affects $C_{n_{\beta,dyn}}$ is the use of static data which do not accurately match flight conditions in calculating $C_{n_{\beta,dyn}}$. Two conditions which may not be matched are control deflections and power. In some cases these parameters can have marked effects on the static lateral-stability parameters C_{n_β} and C_{l_β}.

Another reason for the inability to predict a directional divergence can be seen by examining the curves for C_n and C_l plotted against β. In calculating $C_{n_{\beta,dyn}}$, the curves for C_n and C_l against β are assumed to be linear. This assumption is not always true, especially at high angles of attack. An example of nonlinearity is seen in the case of configuration B (ref. 3). The curves for C_n and C_l against β for the higher angles of attack are shown in figure 7(c). These data show that for $\beta = \pm 2^\circ$ and $\beta = \pm 5^\circ$, C_{l_β} remains negative throughout the angle-of-attack range and C_{n_β} remains positive up to an angle of attack of about 25°, thereby resulting in a curve for $C_{n_{\beta,dyn}}$ that dips at an angle of attack of 25° but does not become negative. However, for $\beta = \pm 10^\circ$, C_{l_β} becomes positive at an angle of attack of about 25° and C_{n_β} becomes negative at an angle of attack of about 22°, thereby resulting in a negative $C_{n_{\beta,dyn}}$ above an angle of attack of 23°. This indicates that both C_{n_β} and C_{l_β} are nonlinear between $\beta = \pm 5^\circ$ and $\beta = \pm 10^\circ$. Free-flight model tests showed that this configuration diverged at an angle of attack of about 25°.

The parameter $C_{n_{\beta,dyn}}$ can also fail to predict a directional divergence when the divergence is caused by the controls. At high angles of attack the rudder may be placed in an area of reduced dynamic pressure in the wake of the wing, thereby resulting in a loss of control power. At the same time, deflection of ailerons at high angles of attack often results in large adverse yawing moments. If these adverse moments become large enough, they may overpower the stability of the aircraft, thereby resulting in a divergence while $C_{n_{\beta,dyn}}$ remains positive. This type of divergence is more fully discussed in reference 7.

METHODS FOR ELIMINATING DIRECTIONAL DIVERGENCE

Since a directional divergence is a very undesirable characteristic for any aircraft, many tests have been made in an effort to determine airframe modifications which would eliminate the divergence. The results presented in table I (refs. 3 to 6 and 8 to 14) show that changes in the airplane configuration can significantly change the airplane's divergence characteristics. In this section the effects of certain airframe modifications on C_{n_β}, C_{l_β}, and consequently on $C_{n_{\beta,dyn}}$ are discussed. The effect of a given modification is shown to vary from aircraft to aircraft, and therefore no general conclusions can be drawn as to the effect of a particular modification.

Increased Vertical-Tail Size

Since a directional divergence is caused by a loss in directional stability, the most obvious airframe modification to improve directional stability would seem to be an increase in the vertical-tail area. In most cases, however, the loss in directional stability is caused by the vertical tail becoming ineffective at high angles of attack because it is in the low-velocity stalled wake of the wing or because it is in a region of adverse sidewash which can even cause the tail to be destabilizing. Under such conditions, increasing the tail area might be destabilizing or at best provide little increase in stability. An example of the effect of increasing the vertical-tail size for configuration C (ref. 4) is shown in figure 8(b). The data show the expected increase in C_{n_β} and C_{l_β} in the lower angle-of-attack range, but there is little effect on the angle of attack at which the derivatives go to zero. Free-flight model tests also showed no difference in the angle of attack at which the divergence occurred with or without the vertical-tail extension. The data of figure 12(b) show the effect of doubling the vertical-tail area of configuration G (ref. 8). These data also show the expected increase in C_{n_β} and C_{l_β} at low angles of attack with the larger vertical tail, but little improvement in the high-angle-of-attack characteristics. Free-flight model tests showed an increase of 3° in the divergence angle for the modified configuration. The data of figure 15(c) show the directional-stability characteristics of configuration J with the short nose (ref. 2) with three different vertical tails. The data show that changes in vertical tail have little effect on C_{n_β} in the high-angle-of-attack range. Free-flight model tests confirm the ineffectiveness of vertical-tail modifications on this configuration in increasing the angle of attack at which the model diverged.

These examples show that increases in vertical-tail area are relatively ineffective in improving the high-angle-of-attack characteristics of the particular configurations studied. It should be pointed out, however, that increased vertical-tail size might be beneficial for other configurations and should be considered before eliminating such a modification as a possible solution to high-angle-of-attack directional-stability deficiencies.

Leading-Edge Slats

One of the most effective means for delaying or eliminating the directional divergence seems to be the leading-edge slat. Force test data show that leading-edge slats result in increases in both C_{n_β} and C_{l_β} (with a corresponding increase in $C_{n_{\beta,dyn}}$), especially in the high-angle-of-attack range. This increase is illustrated in figure 8(b) for configuration C (ref. 4). Free-flight model tests of configuration C showed that leading-edge slats eliminated the directional divergence. Configuration E (fig. 10(b)) shows less of an increase in C_{n_β}, C_{l_β}, and $C_{n_{\beta,dyn}}$ with leading-edge slats than did configuration C, but note that this configuration did not have a divergence problem. Another outstanding example of the effect of leading-edge slats on the high-angle-of-attack characteristics is shown in figure 15(b) for configuration J (ref. 6). The effectiveness of slats in extending the angle of attack of divergence for this configuration has been verified on both free-flight models and flight test aircraft. Both tests showed a 6° increase in the angle of attack at which divergence occurred.

The data presented in figure 21 for configuration P (ref. 9) show the effect of leading-edge slats for two wing sweeps. With a sweep angle of 20° the leading-edge slats produce a large increase in C_{n_β} and C_{l_β}, but for 72° sweep, C_{n_β} is decreased and C_{l_β} is only slightly improved. The effectiveness of the slats seems to be limited by sweep angle.

Although it is not documented in the present paper, experience has shown that leading-edge flaps have effects similar to those of leading-edge slats.

CONCLUSIONS

The present summary of some of the existing data on the directional divergence of high-performance jet airplanes indicates the following:

1. Most high-performance jet aircraft exhibit the directional divergence characteristics.

2. The dynamic directional-stability parameter $C_{n_{\beta,dyn}}$ predicts directional divergence fairly well.

3. Correlation of directional divergence and $C_{n_{\beta,dyn}}$ can be improved by carefully selecting data which represent flight conditions and by accounting for nonlinearity in the curves for yawing moment and rolling moment against angle of sideslip.

4. In some cases a reduction in $C_{n_{\beta,dyn}}$ at high angles of attack to a near zero value may indicate a directional divergence.

5. For aircraft with moderately swept wings, leading-edge slats seem to be the most effective airframe modification for reducing or eliminating the directional divergence potential of the aircraft.

Langley Research Center,
National Aeronautics and Space Administration,
Hampton, Va., October 6, 1972.

APPENDIX

DEVELOPMENT OF $C_{n_{\beta,dyn}}$

The lateral open-loop (no pilot) flight motions are determined by the equation

$$A\lambda^4 + B\lambda^3 + C\lambda^2 + D\lambda + E = 0$$

An aircraft becomes unstable and divergence will occur when one or more of the roots of this equation becomes positive. This equation will have unstable roots if any of the coefficients or if the combination of coefficients $BCD - AD^2 - B^2E$ (Routh's discriminant) becomes negative. Experience has shown directional divergence usually occurs when the C-coefficient becomes negative. The nondimensional form of the equation for the C-coefficient is (ref. 2)

$$C = \mu_b\Big(-K_{X_o}{}^2 C_{Y_r} C_{n_\beta} + K_{X_o}{}^2 C_{n_r} C_{Y_\beta} + 4\mu_b K_{X_o}{}^2 C_{n_\beta} \cos\alpha$$

$$+ K_{Z_o}{}^2 C_{l_p} C_{Y_\beta} - K_{Z_o}{}^2 C_{l_\beta} C_{Y_p} - 4\mu_b K_{Z_o}{}^2 C_{l_\beta} \sin\alpha$$

$$+ \frac{1}{2} C_{n_r} C_{l_p} - \frac{1}{2} C_{n_p} C_{l_r}\Big)$$

By using the definitions

$$\mu_b = \frac{m}{\rho S b}$$

$$K_{X_o}{}^2 = \frac{I_X}{mb^2}$$

and

$$K_{Z_o}{}^2 = \frac{I_Z}{mb^2}$$

and rearranging the terms, the C-coefficient can be reduced to the form

$$C = KC_R$$

where $K = \dfrac{4mI_X}{\rho^2 S^2 b^4}$ is a constant for a given configuration. A change in the sign of the C-coefficient is indicated by a change in the sign of C_R. This reduced form of the C-coefficient is found by the equation

$$C_R = C_{n_\beta}\left(\cos\alpha - \frac{\rho Sb}{4m}C_{Y_r}\right) - \frac{I_Z}{I_X}C_{l_\beta}\left(\sin\alpha + \frac{\rho Sb}{4m}C_{Y_p}\right)$$

$$+ \frac{\rho Sb}{4I_X}C_{l_p}\left(\frac{b^2}{2}C_{n_r} + \frac{I_Z}{m}C_{Y_\beta}\right) + \frac{\rho Sb}{4}\left(\frac{1}{m}C_{n_r}C_{Y_\beta} - \frac{b^2}{2I_X}C_{l_r}C_{n_p}\right)$$

This equation shows that most of the terms are the product of two derivatives. These derivatives are usually <<1; therefore the products of these derivatives are assumed to be small compared to the other terms. Terms involving products of derivatives are dropped from the equations, thereby yielding the equation

$$C_R' = C_{n_\beta}\cos\alpha - \frac{I_Z}{I_X}C_{l_\beta}\sin\alpha$$

This equation has been further reduced by assuming $\cos\alpha = 1$. The resulting expression is called $C_{n_{\beta,dyn}}$ because it is an indication of dynamic directional stability. Thus

$$C_{n_{\beta,dyn}} = C_{n_\beta} - \frac{I_Z}{I_X}C_{l_\beta}\sin\alpha$$

This last assumption can be shown to have little effect on the results. Calculations have been made for two different configurations to compare the values of C_R, C_R', and $C_{n_{\beta,dyn}}$, that is, to illustrate the effect of the simplifications. The calculations were done in terms of per radian to fit the equation for C. The results of these calculations are presented in figure 23. These results show that $C_{n_{\beta,dyn}}$ is a good representation of C_R.

REFERENCES

1. Mechtly, E. A.: The International System of Units – Physical Constants and Conversion Factors (Revised). NASA SP-7012, 1969.

2. Chambers, Joseph R.; and Anglin, Ernie L.: Analysis of Lateral-Directional Stability Characteristics of a Twin-Jet Fighter Airplane at High Angles of Attack. NASA TN D-5361, 1969.

3. Johnson, Joseph L., Jr.; and Boisseau, Peter C.: Investigation of the Low-Speed Stability and Control Characteristics of a 1/10-Scale Model of the Convair YF-102 Airplane in the Langley Free-Flight Tunnel. NACA RM SL53L04, U.S. Air Force, 1953.

4. Johnson, Joseph L., Jr.: Investigation of the Low-Speed Stability and Control Characteristics of a 1/10-Scale Model of the Douglas XF4D-1 Airplane in the Langley Free-Flight Tunnel – TED No. NACA DE 349, NACA RM SL51J22, Bur. Aeronaut., 1951.

5. Tosti, Louis P.; and Bates, William R.: Flight Characteristics at Low Speed of a 1/12-Scale Model of the Consolidated Vultee 7002 Airplane (Flying Mock-Up of XP-92). NACA RM SL8B12, U.S. Air Force, 1948.

6. Newsom, William A., Jr.; and Grafton, Sue B.: Free-Flight Investigation of Effects of Slats on Lateral-Directional Stability of a 0.13-Scale Model of the F-4E Airplane – COORD No. AF-AM-113. NASA TM SX-2337, U.S. Air Force, 1971.

7. Moul, Martin T.; and Paulson, John W.: Dynamic Lateral Behavior of High-Performance Aircraft. NACA RM L58E16, 1958.

8. McKinney, Marion O.; and Smith, Charles C., Jr.: Low-Speed Wind-Tunnel Tests of a 1/8-Scale Model of the Bell D-188A VTOL Airplane – TED No. NACA AD 3147. NACA RM SL58H15, Bur. Aeronaut., 1958.

9. Freeman, Delma C., Jr.: Low Subsonic Flight and Force Investigation of a Supersonic Transport Model With a Variable-Sweep Wing. NASA TN D-4726, 1968.

10. Boisseau, Peter C.: Investigation of the Low-Speed Stability and Control Characteristics of a 1/7-Scale Model of the North American X-15 Airplane. NACA RM L57D09, 1957.

11. Burris, W. R.; and Hutchins, D. E.: Effect of Wing Leading Edge Geometry on Maneuvering Boundaries and Stall Departure. AIAA Paper No. 70-904, July 1970.

12. Paulson, John W.: Investigation of the Low-Speed Flight Characteristics of a 1/15-Scale Model of the Convair XB-58 Airplane – COORD No. AF-AM-15. NACA RM SL57K19, U.S. Air Force, 1957.

13. Freeman, Delma C., Jr.: Low-Subsonic Flight and Force Investigation of a Supersonic Transport Model With a Double-Delta Wing. NASA TN D-4179, 1968.

14. Freeman, Delma C., Jr.: Low Subsonic Flight and Force Investigation of a Supersonic Transport Model With a Highly Swept Arrow Wing. NASA TN D-3887, 1967.

TABLE I.- CORRELATION OF $C_{n_{\beta,dyn}}$ WITH FLIGHT TEST RESULTS

Configuration	Description	I_Z/I_X	Angle of attack for divergence, deg			Correlation	Reference
			$C_{n_{\beta,dyn}} = 0$	Model flight test	Full-scale flight test		
A	Basic	6.61	No divergence	No divergence	----------	Good	5
B	Basic	6.29	22.5	25	----------	Fair	3
C	Basic	4.34	22.5	20	----------	Good	4
	Vertical-tail extension	4.34	23	20	----------	Good	
	Leading-edge slats	4.34	No divergence	No divergence	----------	Good	
D	Basic	11.20	No divergence	26	Diverges	Poor	Unpublished data
E	Basic	3.46	No divergence	----------	No divergence	Good	Unpublished data
	Leading-edge slats	3.46	No divergence	----------	No divergence	Good	
F	Basic	2.90	19.5	----------	Diverges	Fair[a]	Unpublished data
G	Basic	4.70	15.2	Diverges	----------	Good	8
	Large-vertical tail	4.70	16.2	Diverges	----------	Good	
H	Basic	19.62	28.8	30	----------	Good	10
I	Basic	4.40	25	----------	Diverges	Good	11 and unpublished data
J	Basic	8.42	24.8	26	Diverges	Good	2 and 6
	Leading-edge slats	8.42	[b]33	32	Diverges	Fair	
K	Basic, $\Lambda = 26^o$	5.14	26.8	25	Diverges	Good	Unpublished data
	Basic, $\Lambda = 72.5^o$	10.46	34.8	32	----------	Good	
L	Basic	11.03	No divergence	No divergence	No divergence	Good	Unpublished data
M	Basic	3.62	28.2	30	Diverges	Good	12
	Bomb pod	3.67	28	30	Diverges	Good	
N	Inboard vertical tails	21.91	37.3	40 to 45	----------	Fair	Unpublished data
	Outboard vertical tails	21.91	[b]40	40 to 45	----------	Fair	
O	Basic	8.98	26.6	28	----------	Good	13
	Leading-flap	9.87	28.6	28	----------	Good	
P	Leading-edge slats, $\Lambda = 20^o$	4.23	No divergence	27	----------	Poor	9
	Leading-edge slats, $\Lambda = 72^o$	8.33	No divergence	22	----------	Poor	
Q	Basic	7.46	No divergence	No divergence	----------	Good	14
	Canard	7.43	No divergence	No divergence	----------	Good	

[a] Data from uninstrumented aircraft.

[b] Angle at which $C_{n_{\beta,dyn}}$ dips toward but does not reach zero.

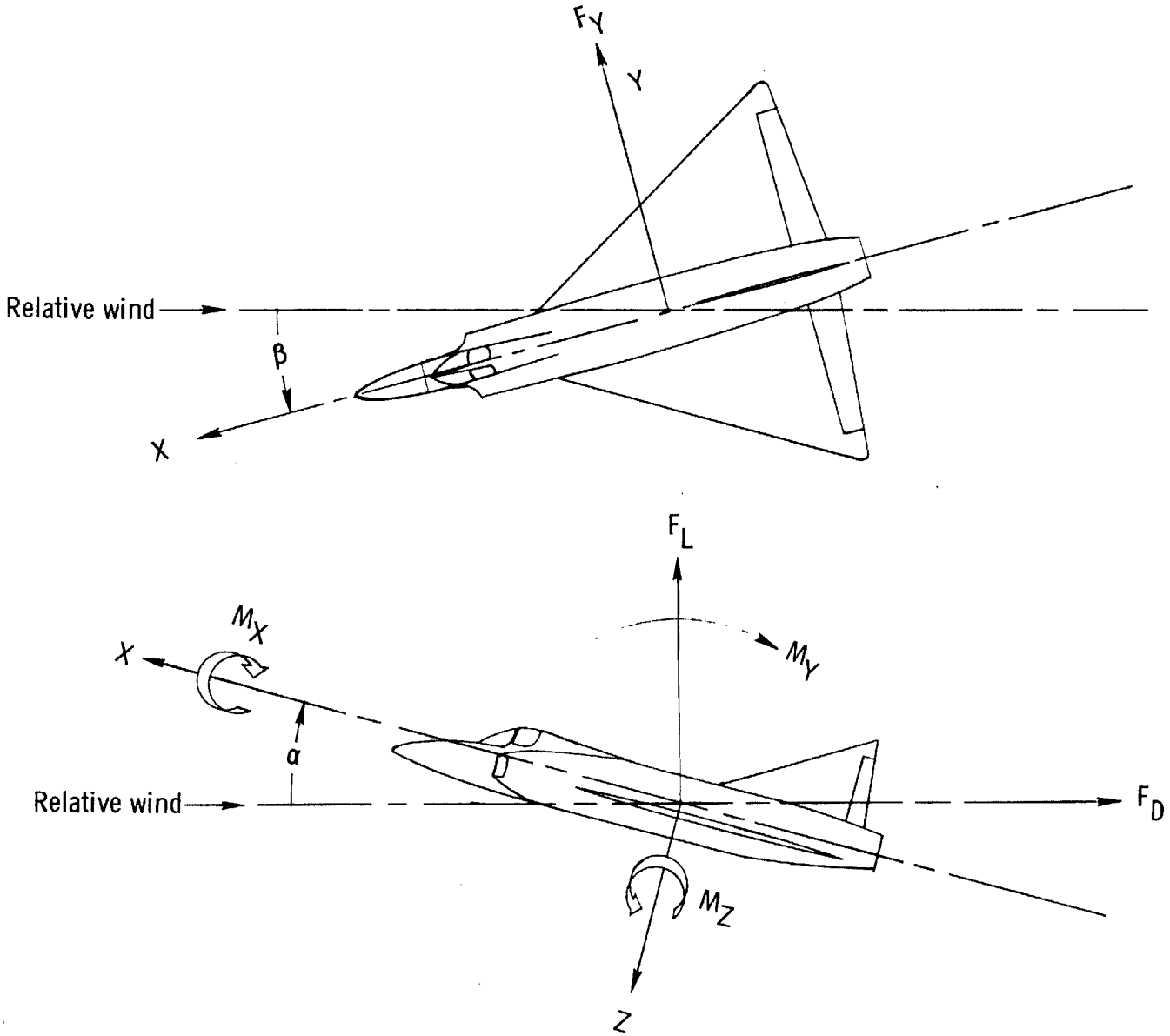

Figure 1.- System of axes used in investigation. Longitudinal data are referred to wind axis, and lateral data are referred to body axes. Arrows indicate positive directions of moments, forces, and angles.

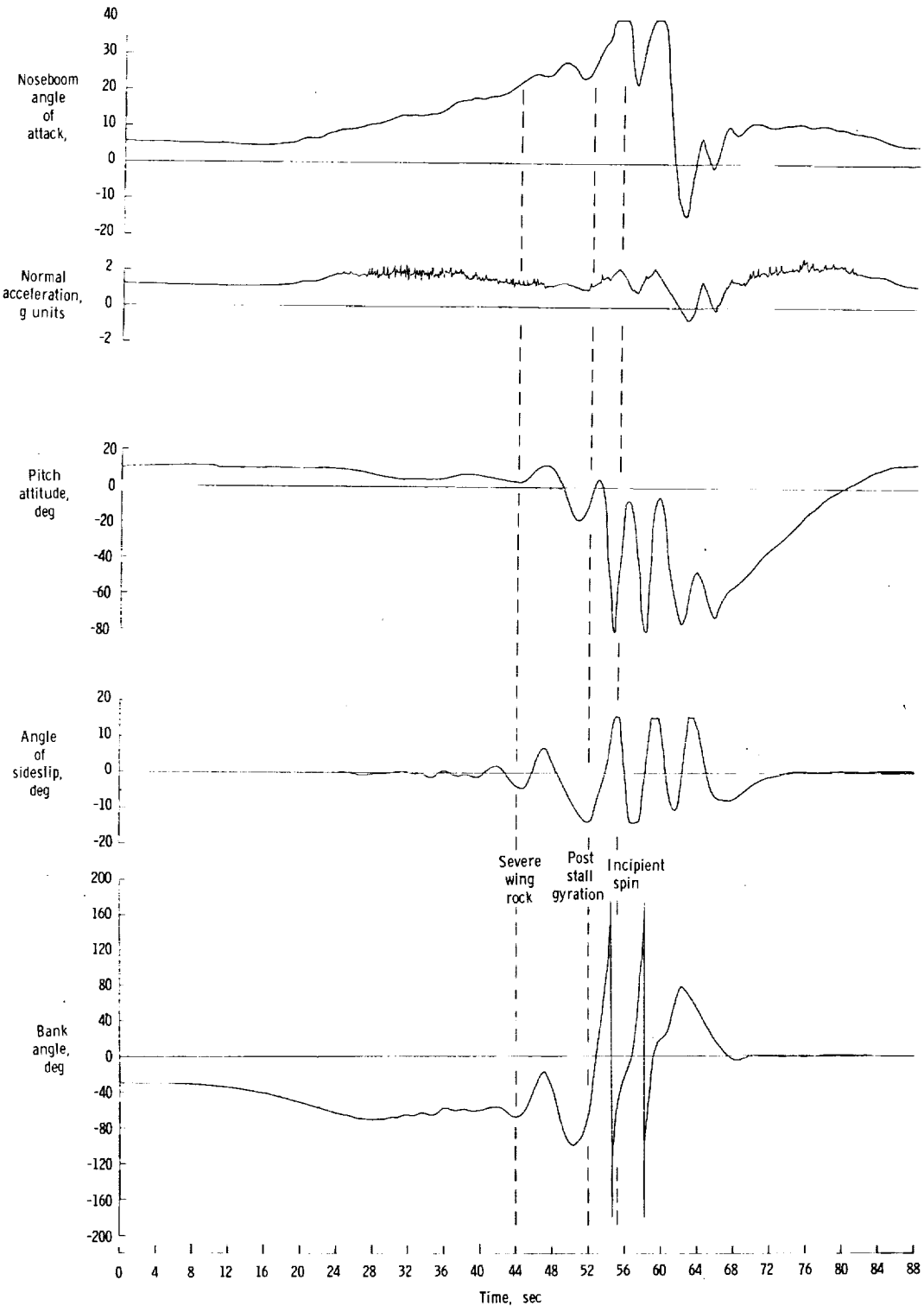

(a) Flight variables.

Figure 2.- Time histories of directional divergence encountered in flight. Configuration J.

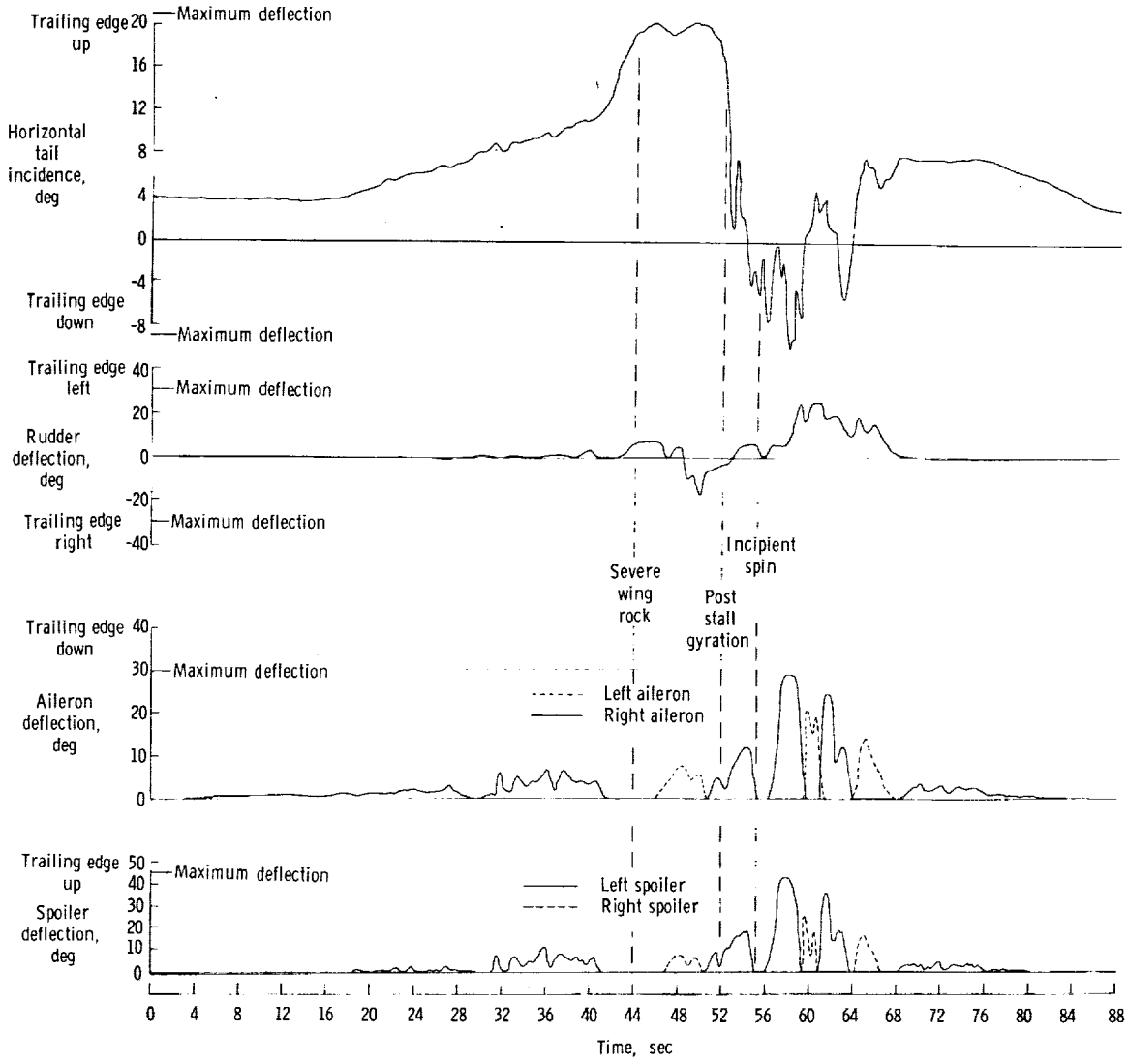

(b) Control-surface deflections.

Figure 2.- Concluded.

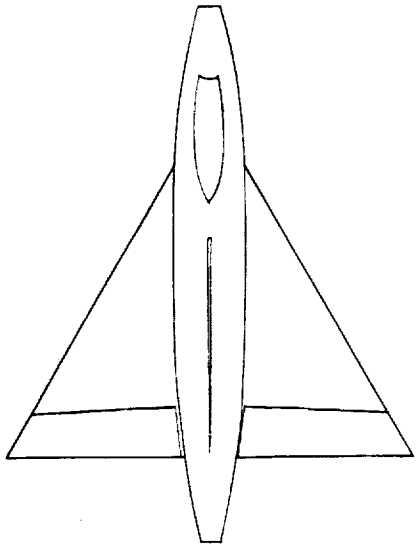

Configuration A
(ref. 5)

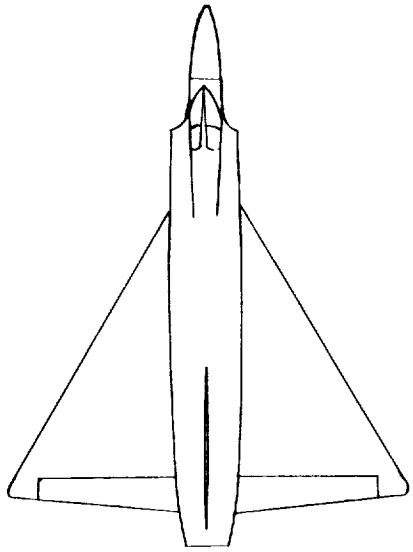

Configuration B
(ref. 3)

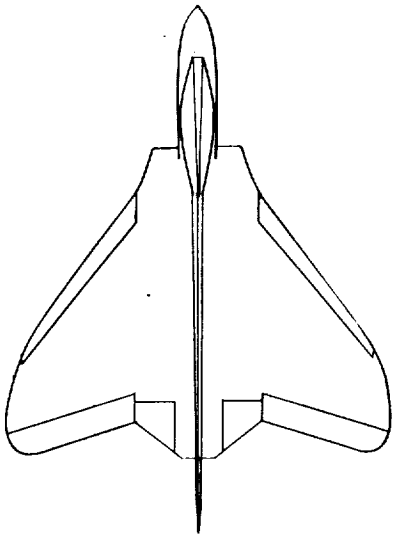

Configuration C
(ref. 4)

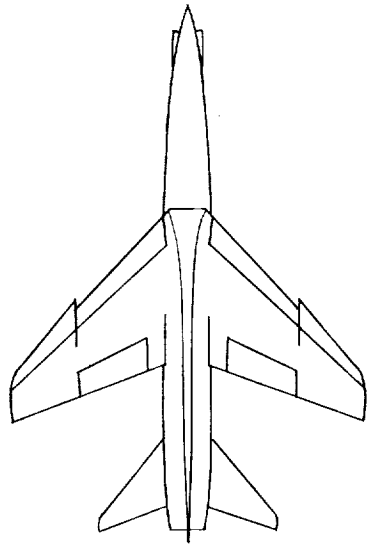

Configuration D
(unpublished data)

Figure 3.- Plan view of fighter configurations examined in study.

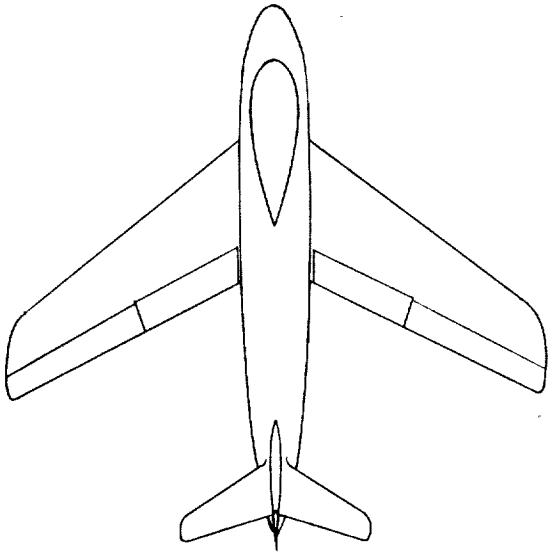

Configuration E
(unpublished data)

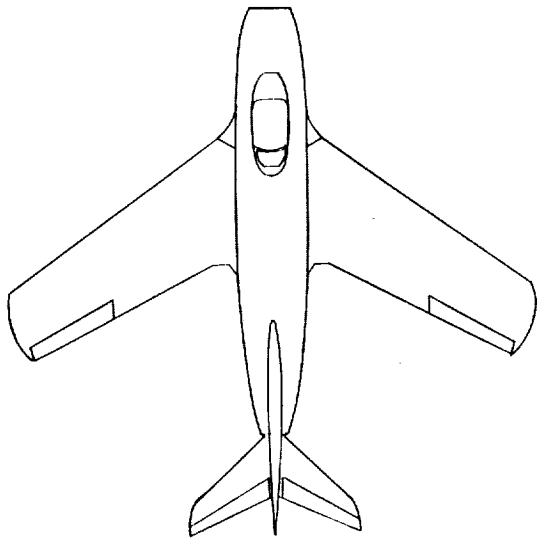

Configuration F
(unpublished data)

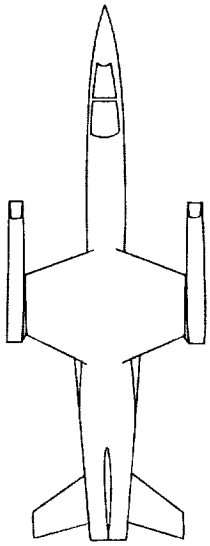

Configuration G
(ref. 8)

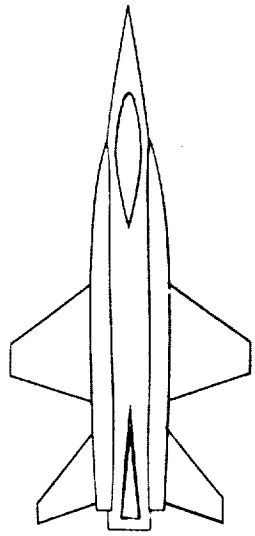

Configuration H
(ref. 10)

Figure 3.- Continued.

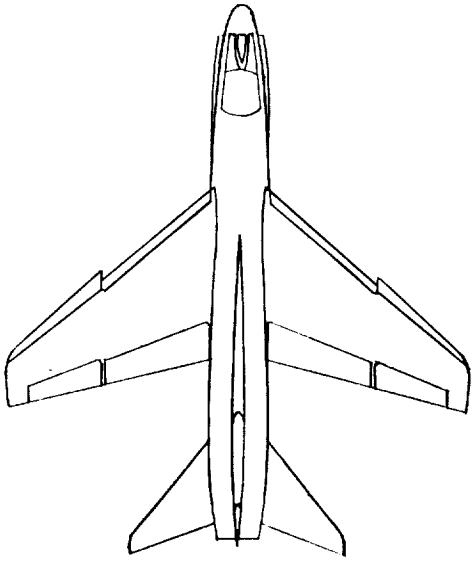

Configuration I
(ref. 11 and unpublished data)

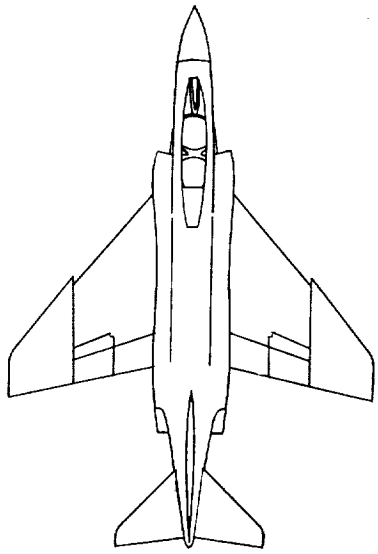

Configuration J
(refs. 2 and 6)

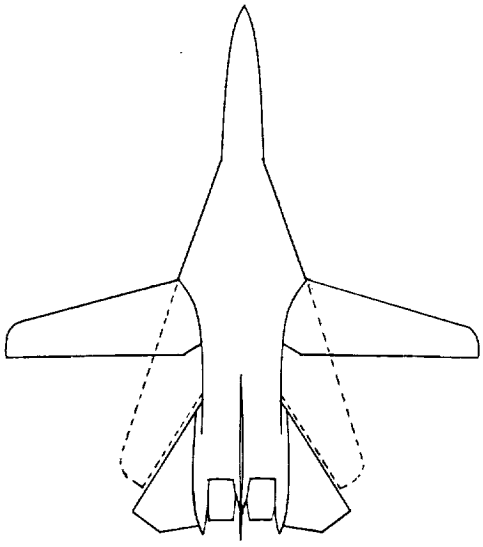

Configuration K
(unpublished data)

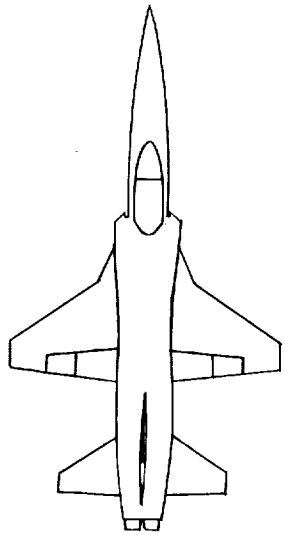

Configuration L
(unpublished data)

Figure 3.- Concluded.

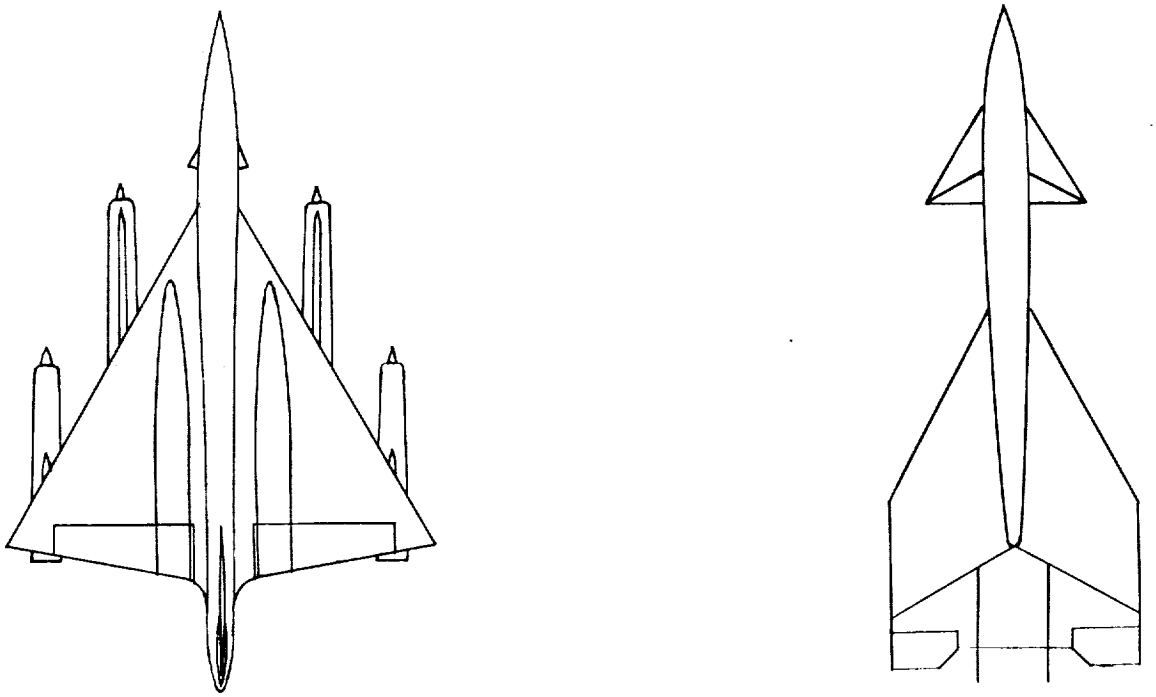

Configuration M
(ref. 12)

Configuration N
(unpublished data)

Figure 4.- Plan view of bomber configurations examined in study.

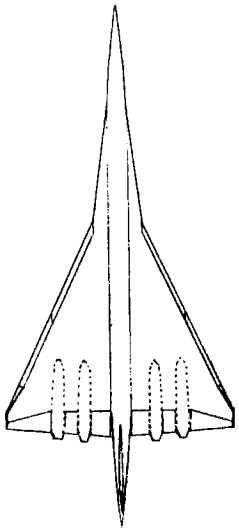

Configuration O
(ref. 13)

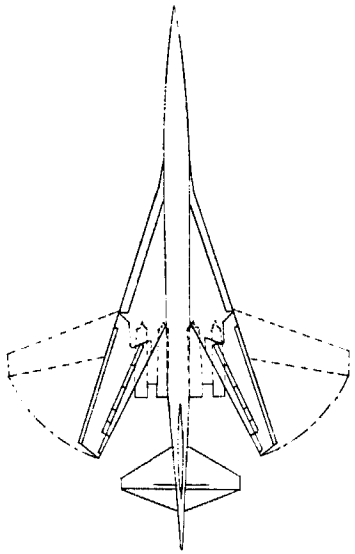

Configuration P
(ref. 9)

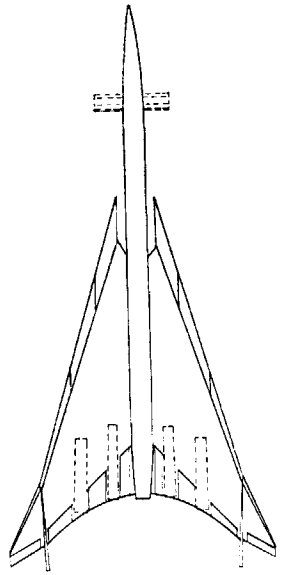

Configuration Q
(ref. 14)

Figure 5.- Plan view of transport configurations examined in study.

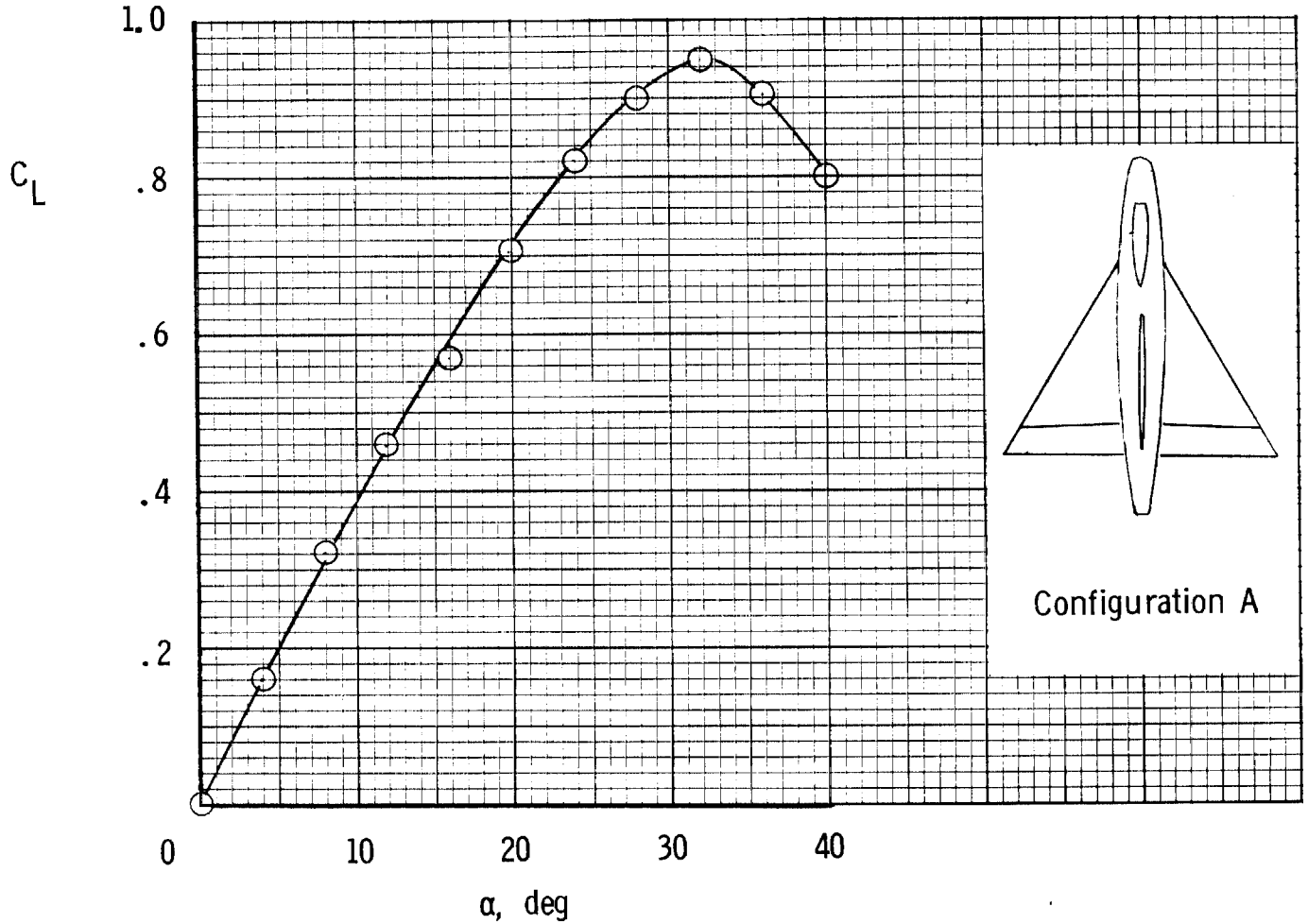

(a) Longitudinal characteristics.

Figure 6.- Longitudinal and lateral characteristics of configuration A (ref. 5).

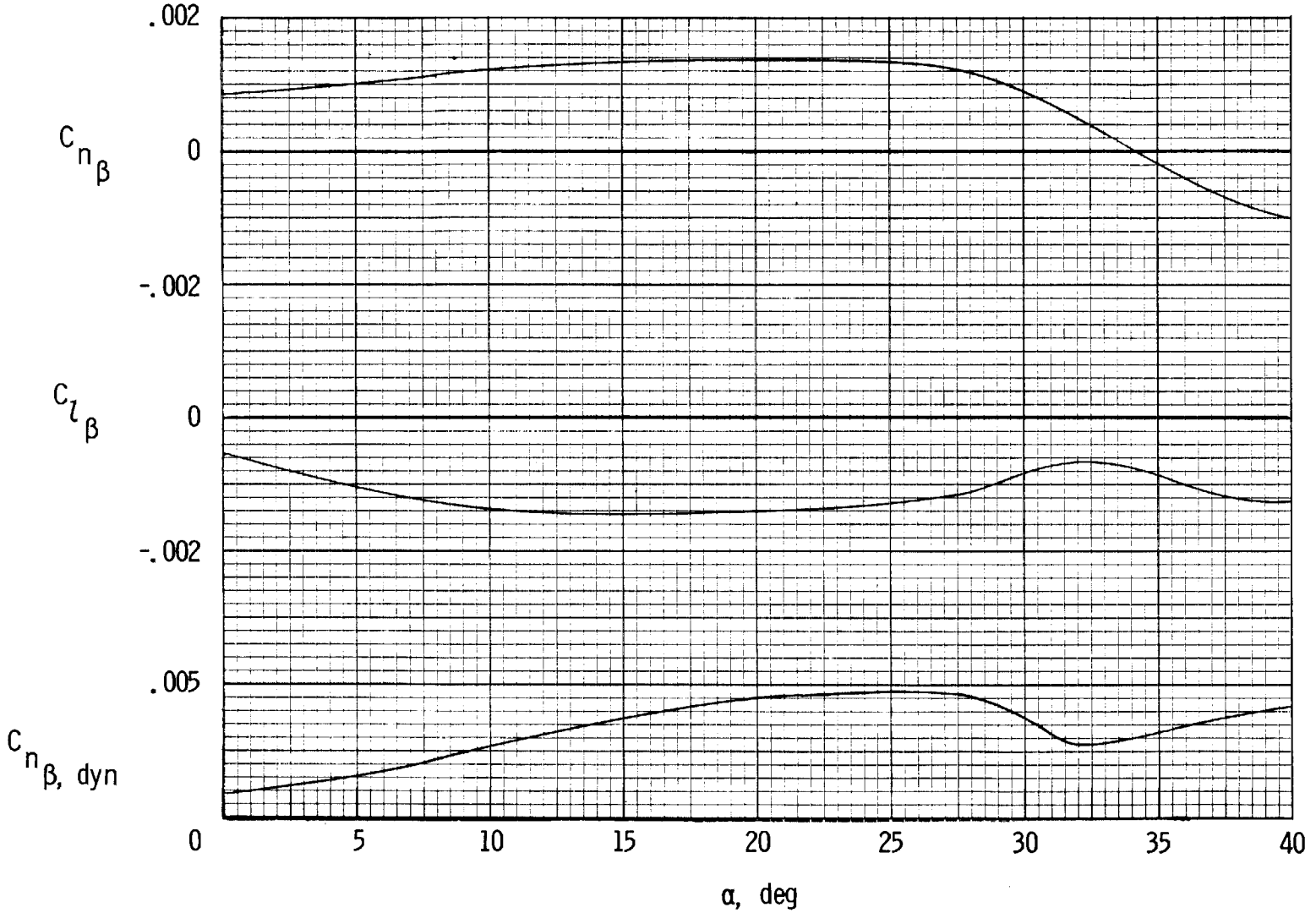

(b) Lateral characteristics. $\beta = \pm 5^{o}$.

Figure 6.- Concluded.

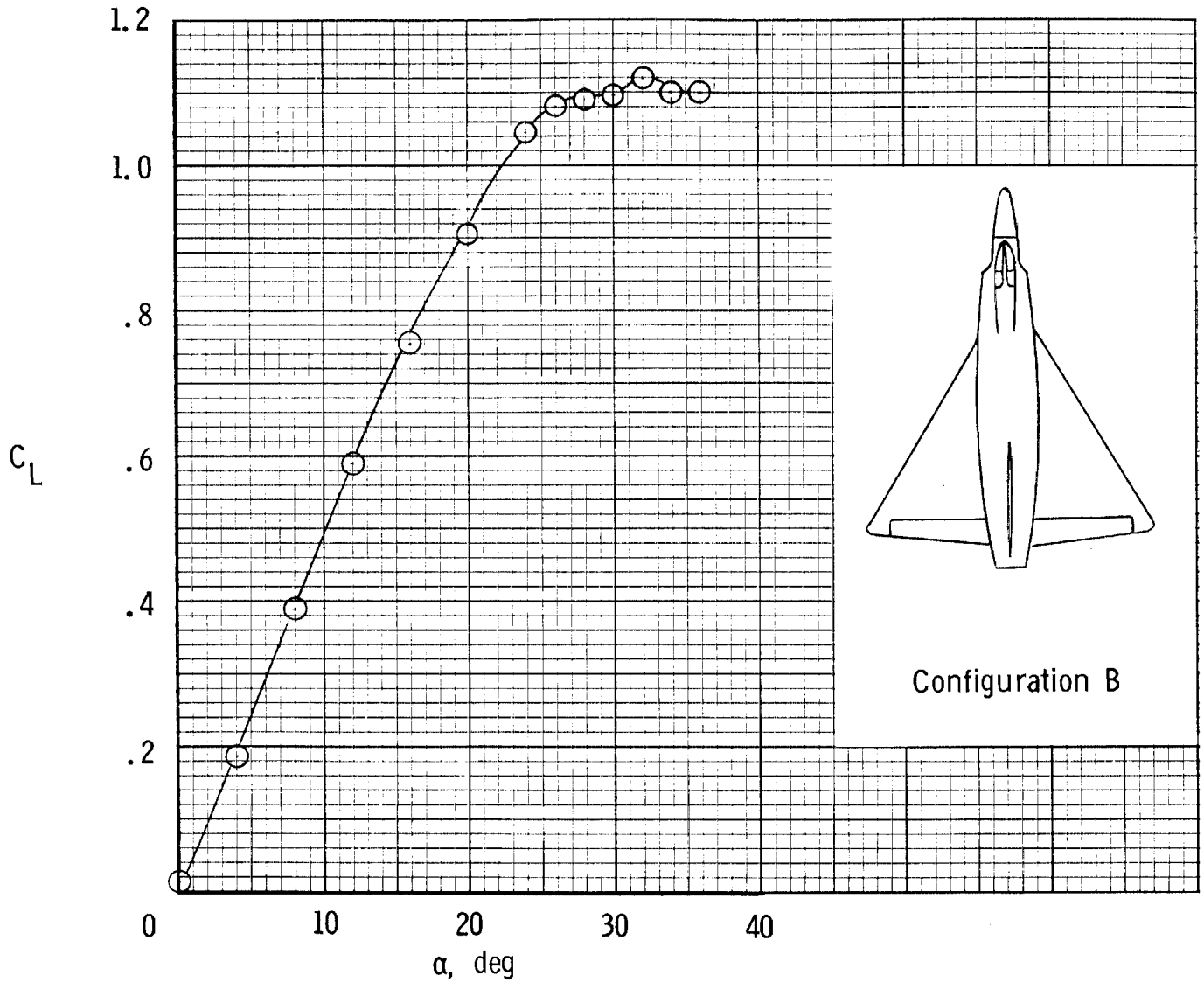

(a) Longitudinal characteristics.

Figure 7.- Longitudinal and lateral characteristics of configuration B (ref. 3).

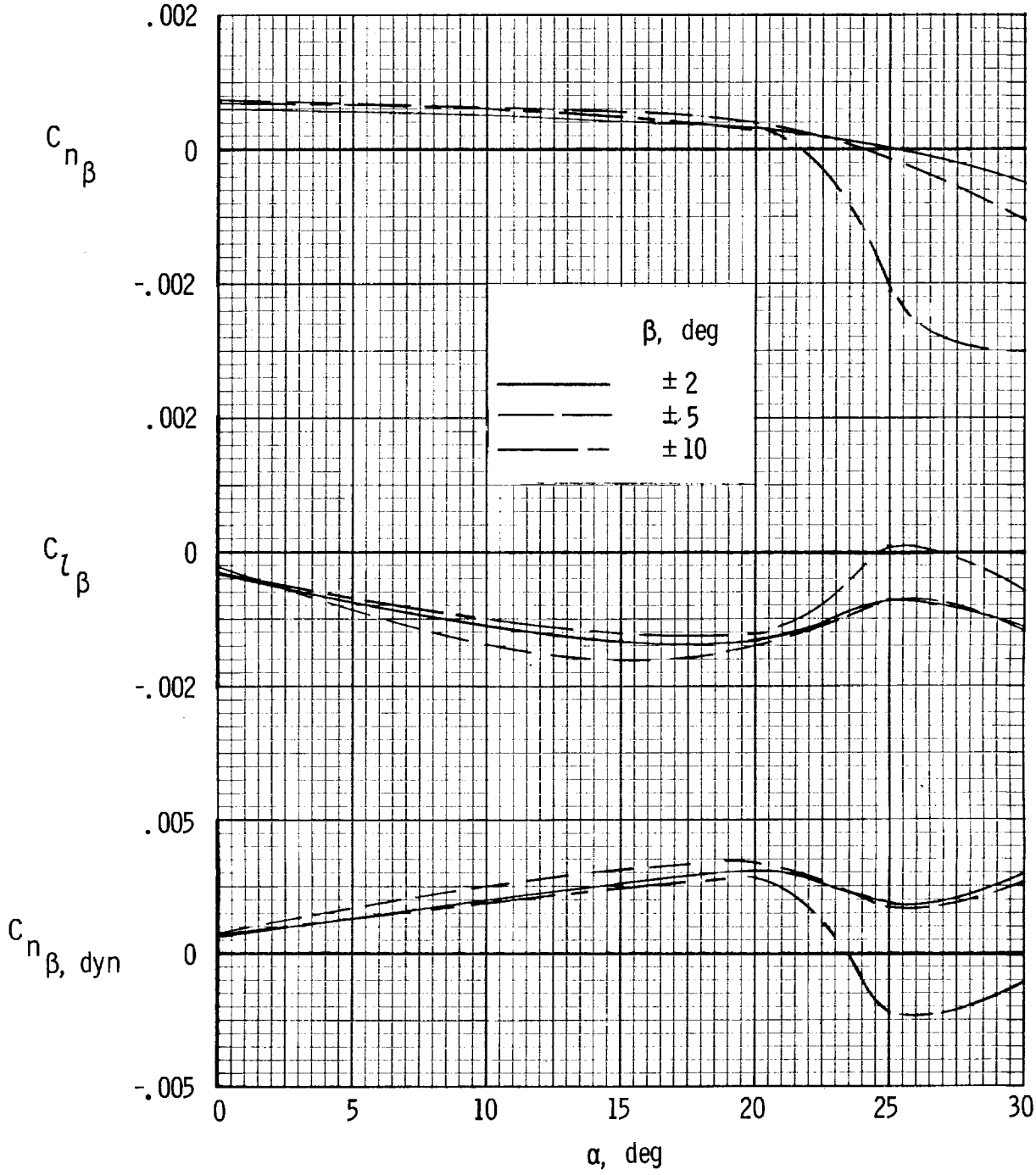

(b) Lateral characteristics.

Figure 7.- Continued.

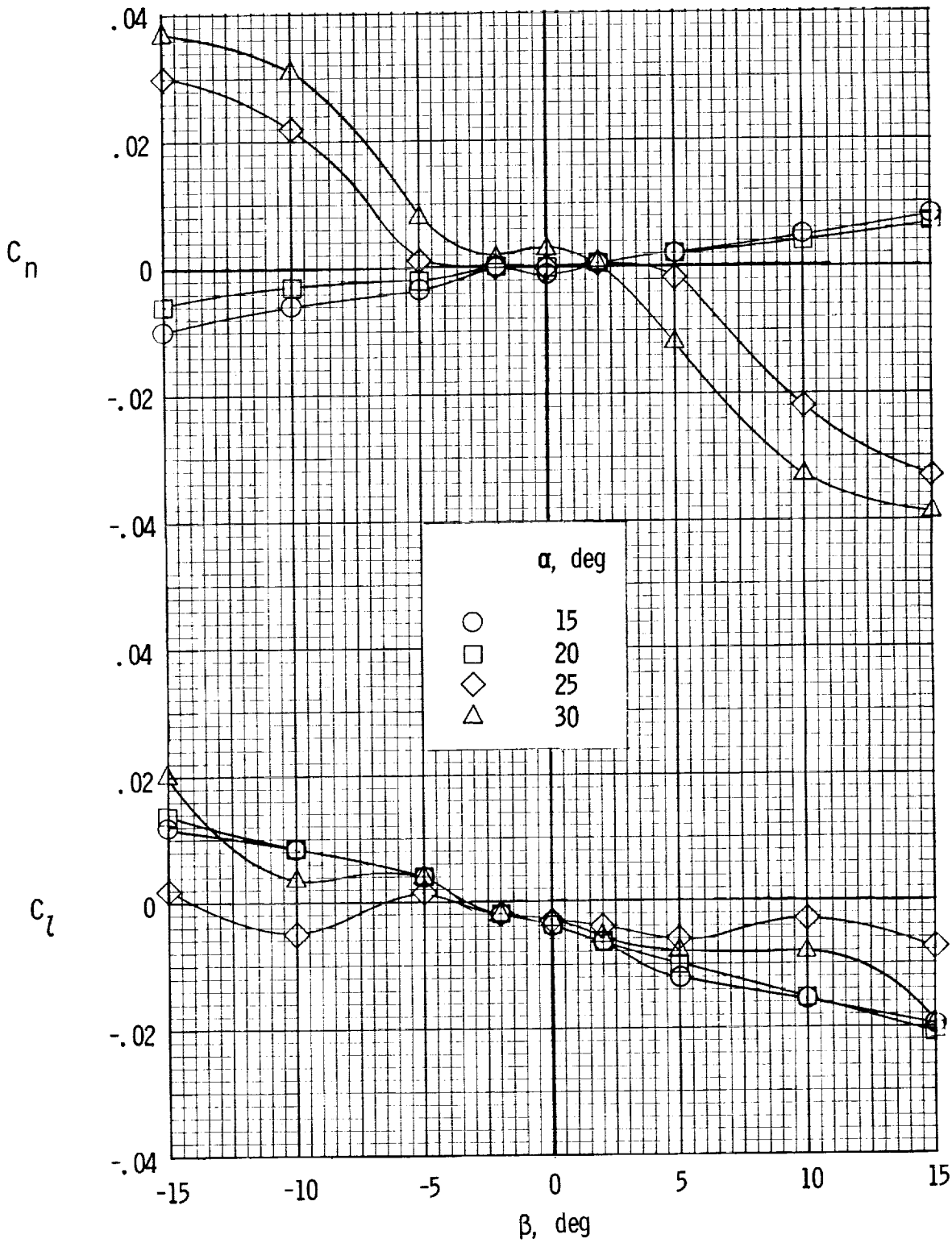

(c) Variation of lateral characteristics with sideslip.

Figure 7.- Concluded.

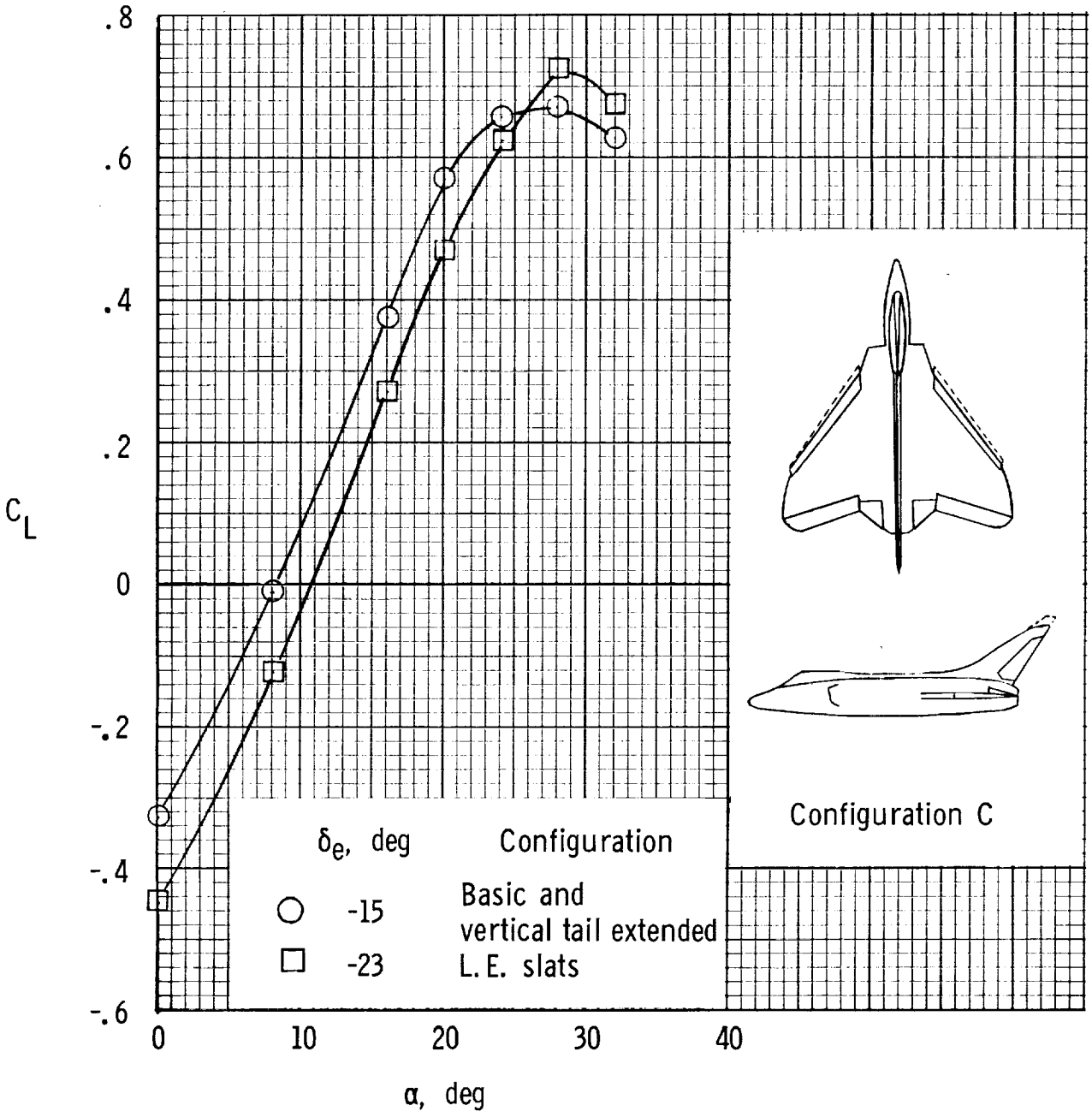

(a) Longitudinal characteristics.

Figure 8.- Longitudinal and lateral characteristics of configuration C (ref. 4).

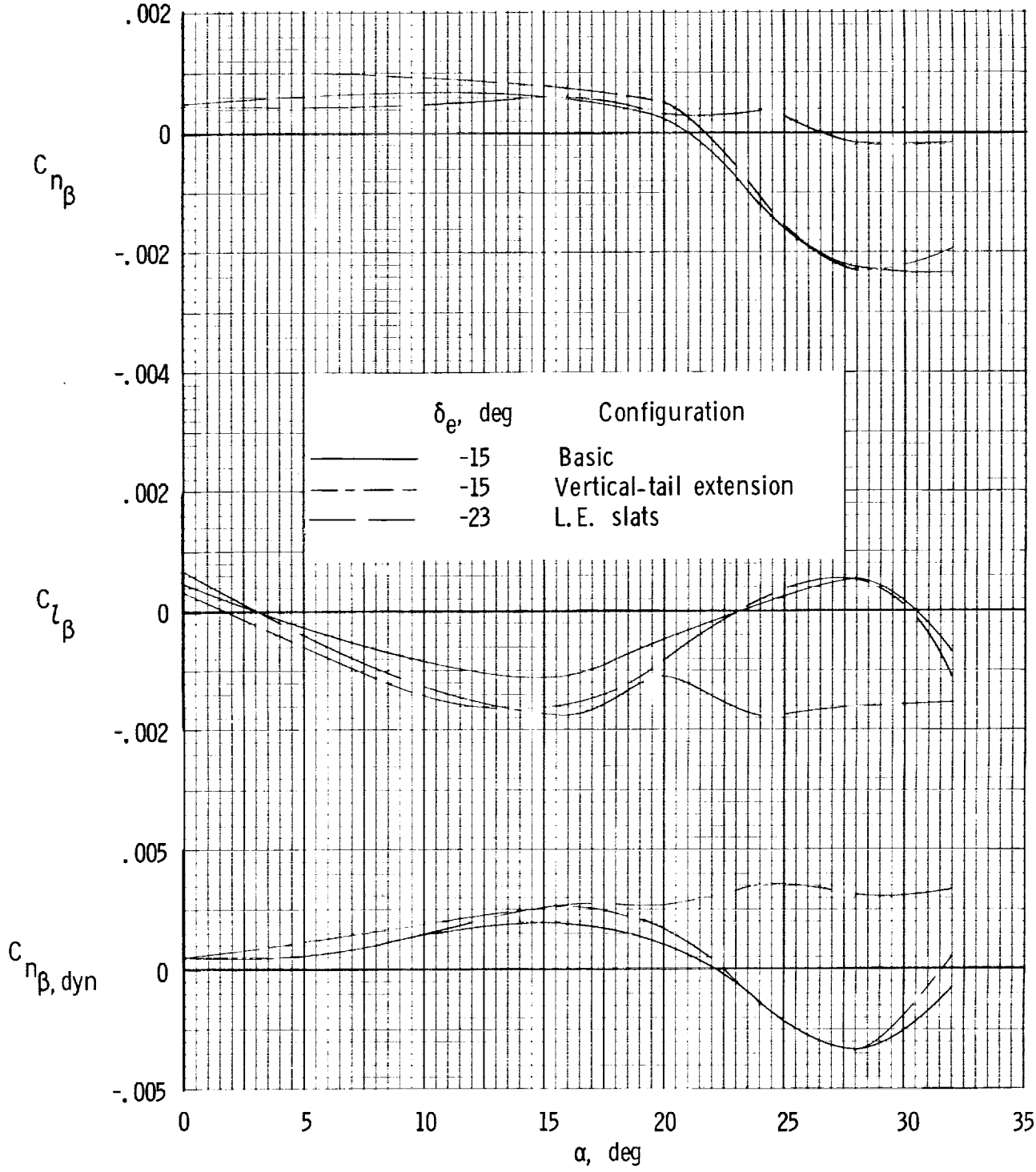

(b) Lateral characteristics. $\beta = \pm 5^{o}$.

Figure 8.- Concluded.

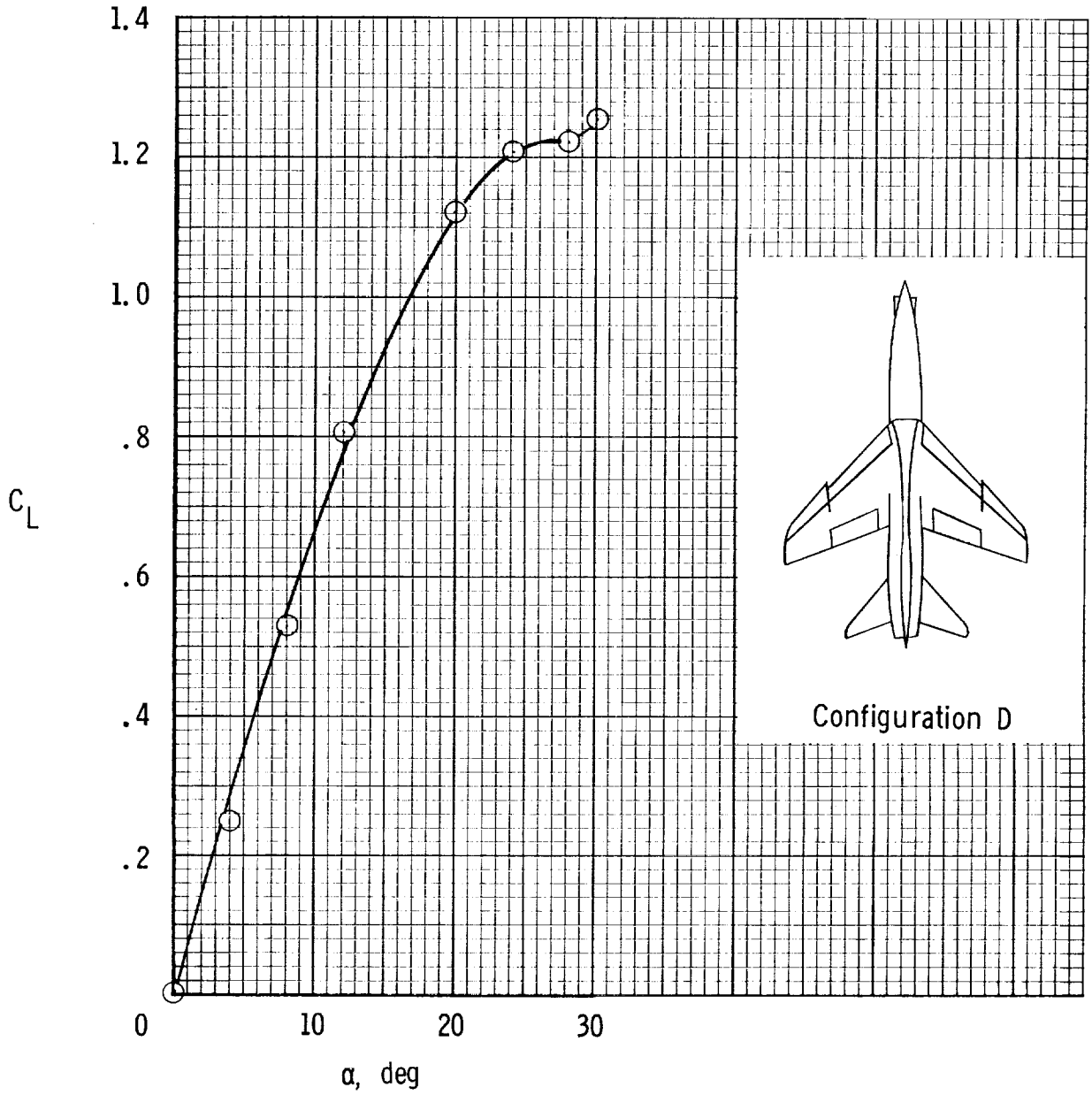

(a) Longitudinal characteristics.

Figure 9.- Longitudinal and lateral characteristics of configuration D (unpublished data).

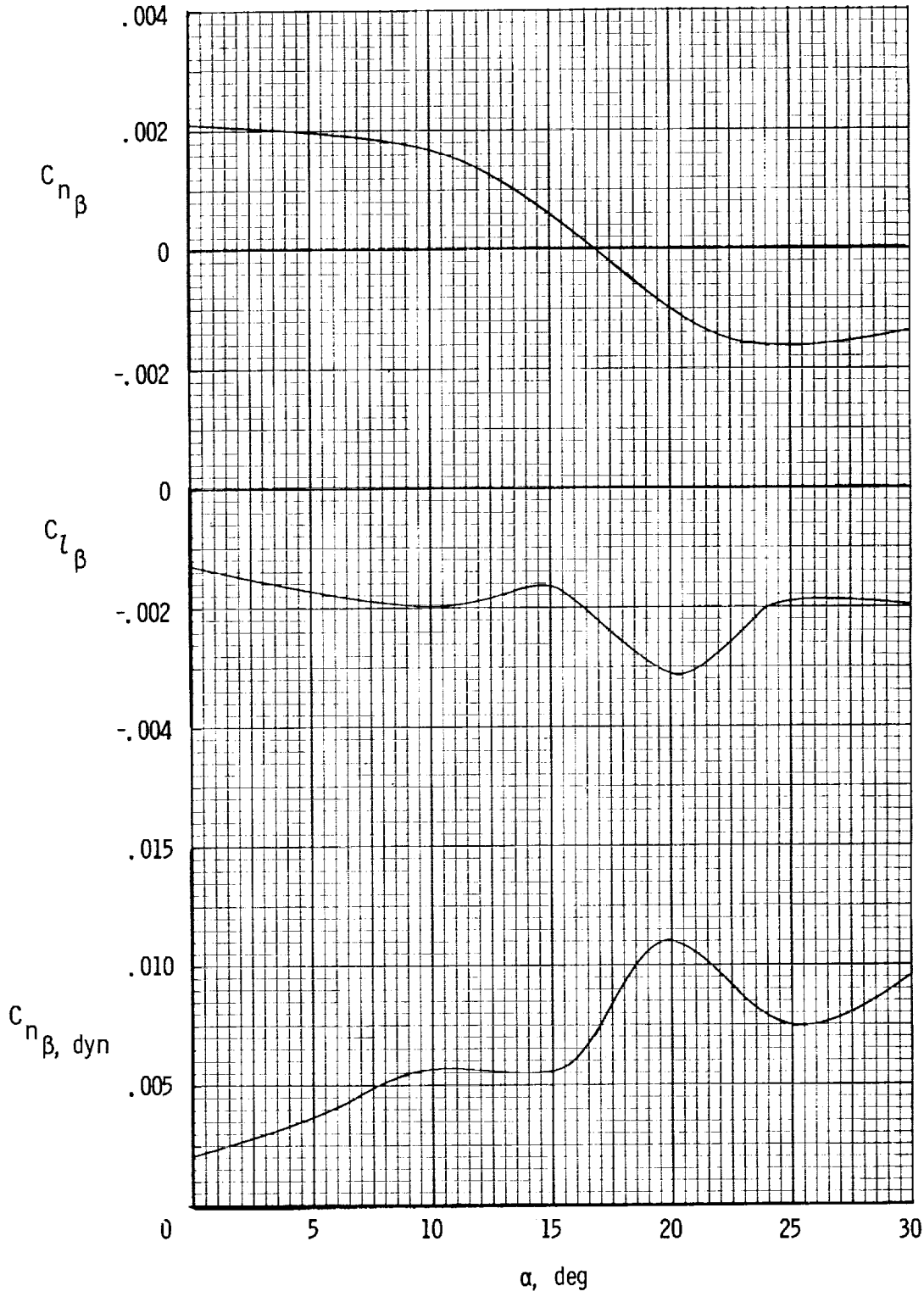

(b) Lateral characteristics. $\beta = \pm 5^{o}$.

Figure 9.- Concluded.

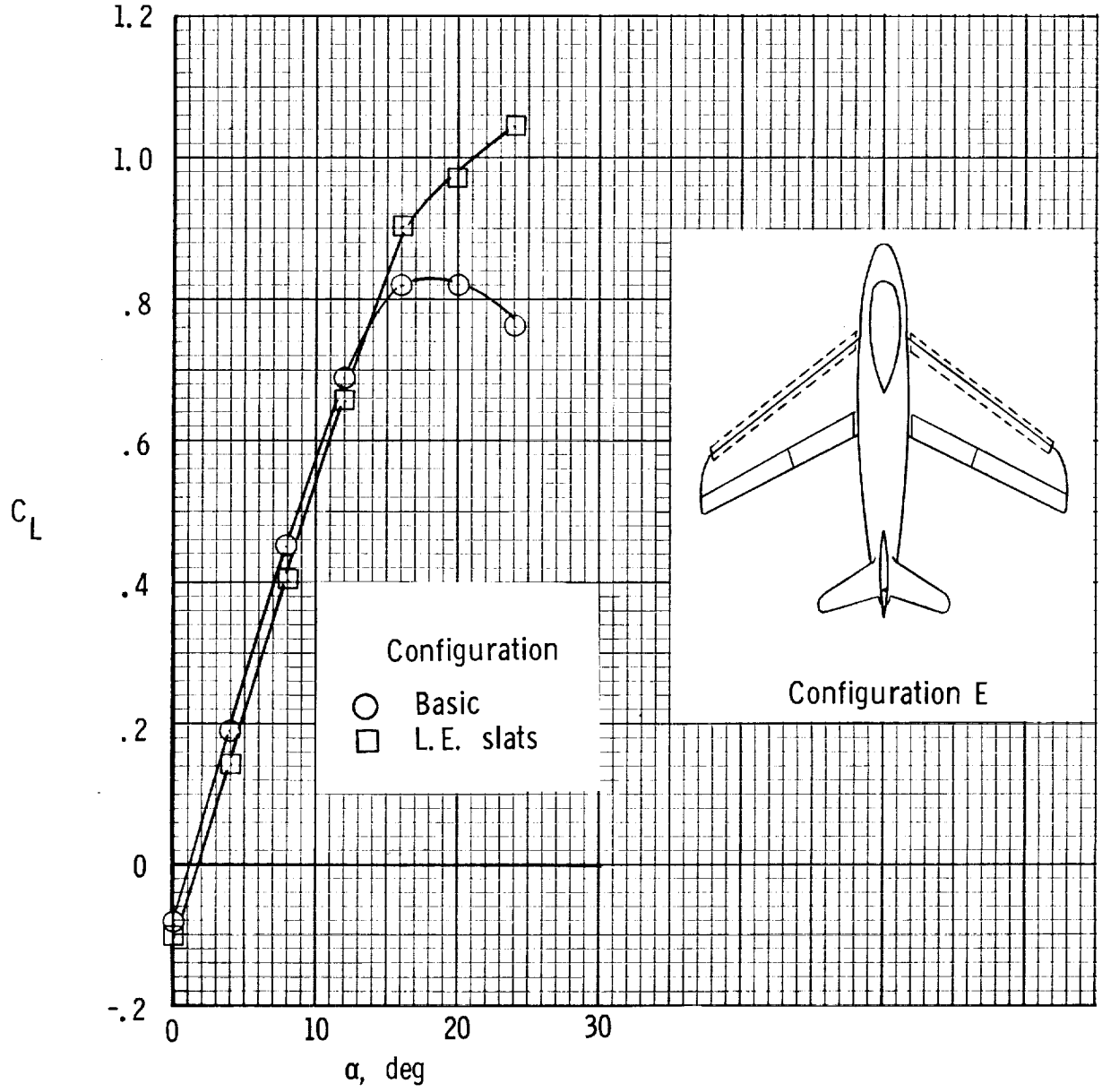

(a) Longitudinal characteristics.

Figure 10.- Longitudinal and lateral characteristics of configuration E (unpublished data).

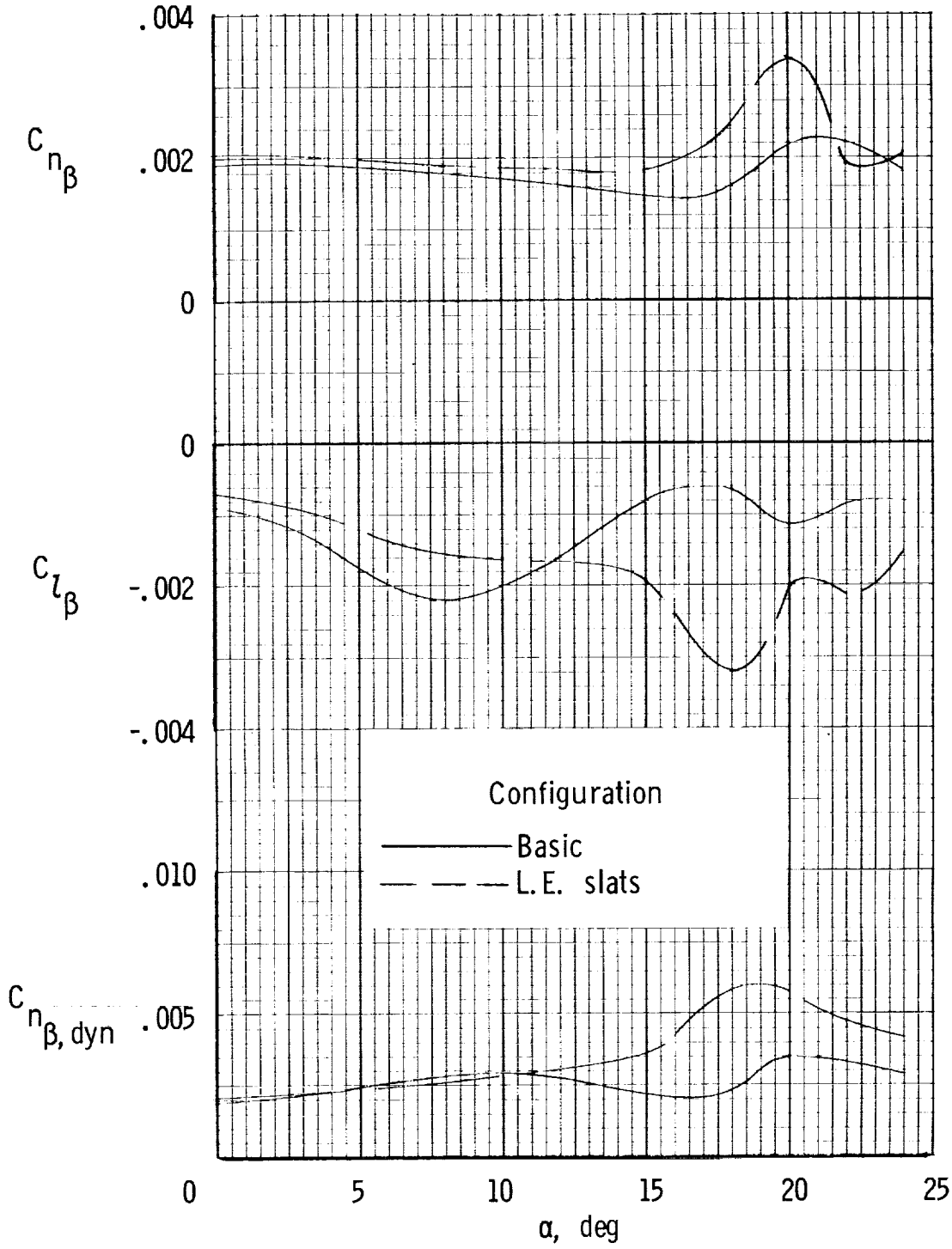

(b) Lateral characteristics. $\beta = \pm 5^{o}$.

Figure 10.- Concluded.

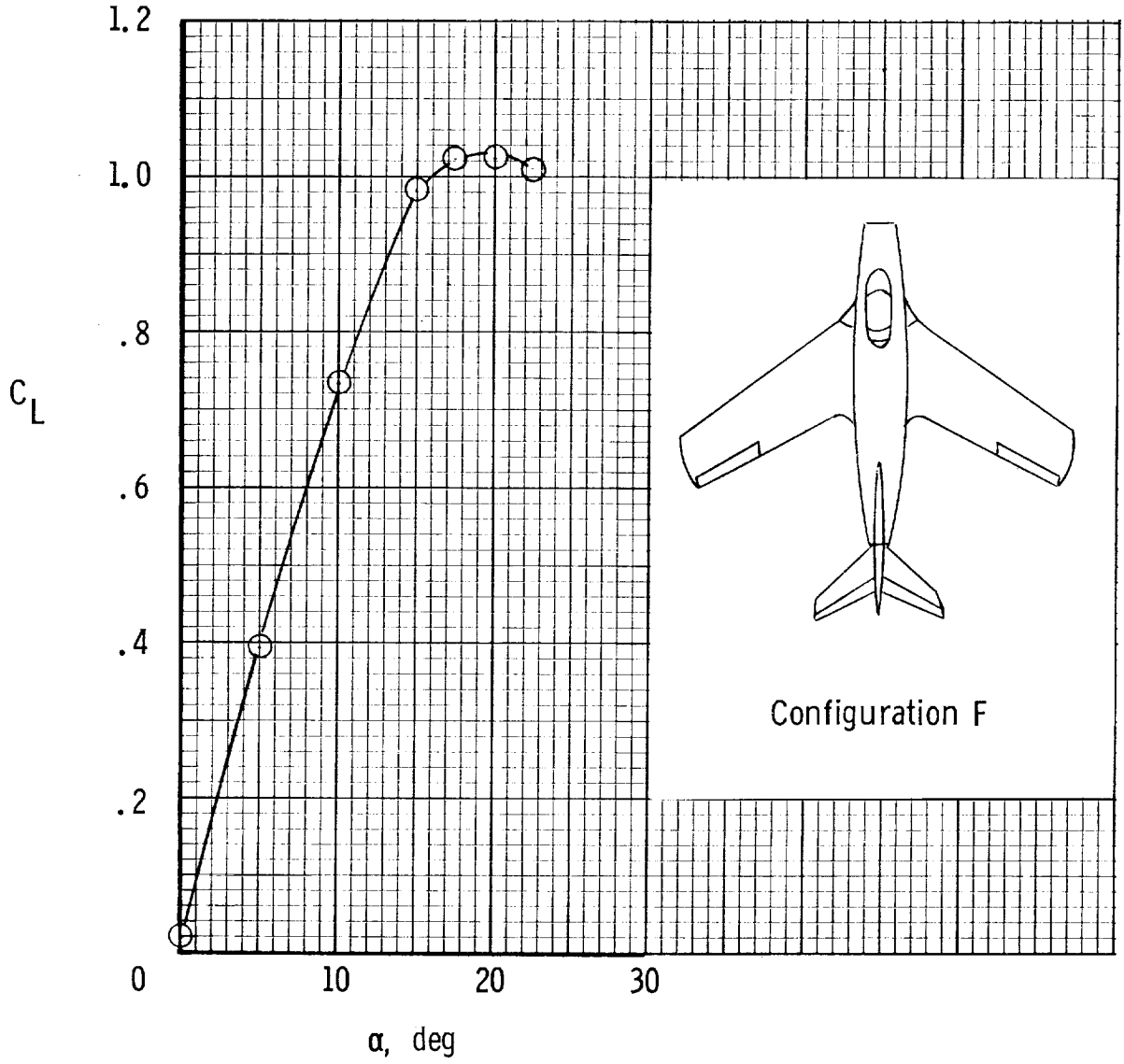

(a) Longitudinal characteristics.

Figure 11.- Longitudinal and lateral characteristics of configuration F (unpublished data).

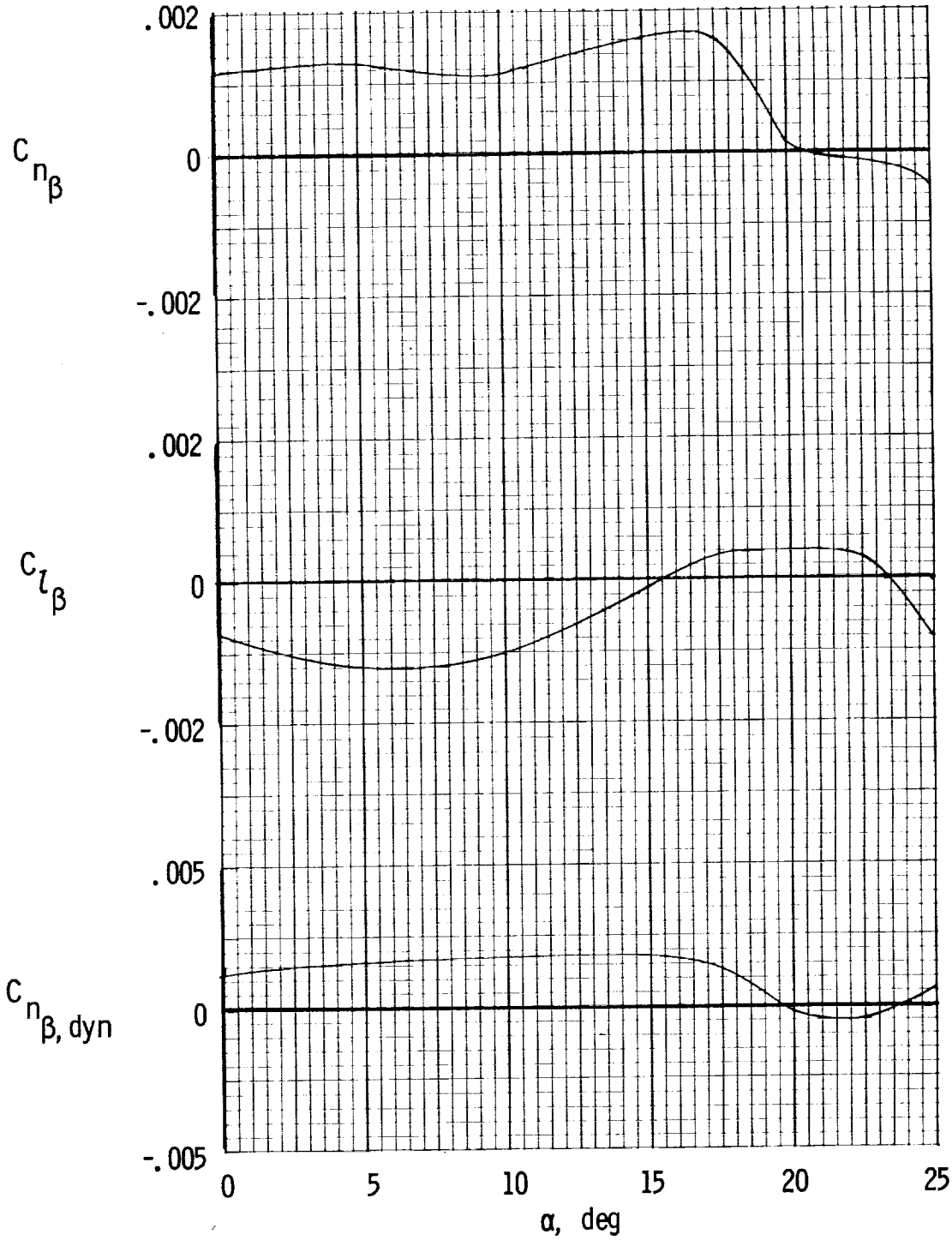

(b) Lateral characteristics. $\beta = \pm 5^{\circ}$.

Figure 11.- Concluded.

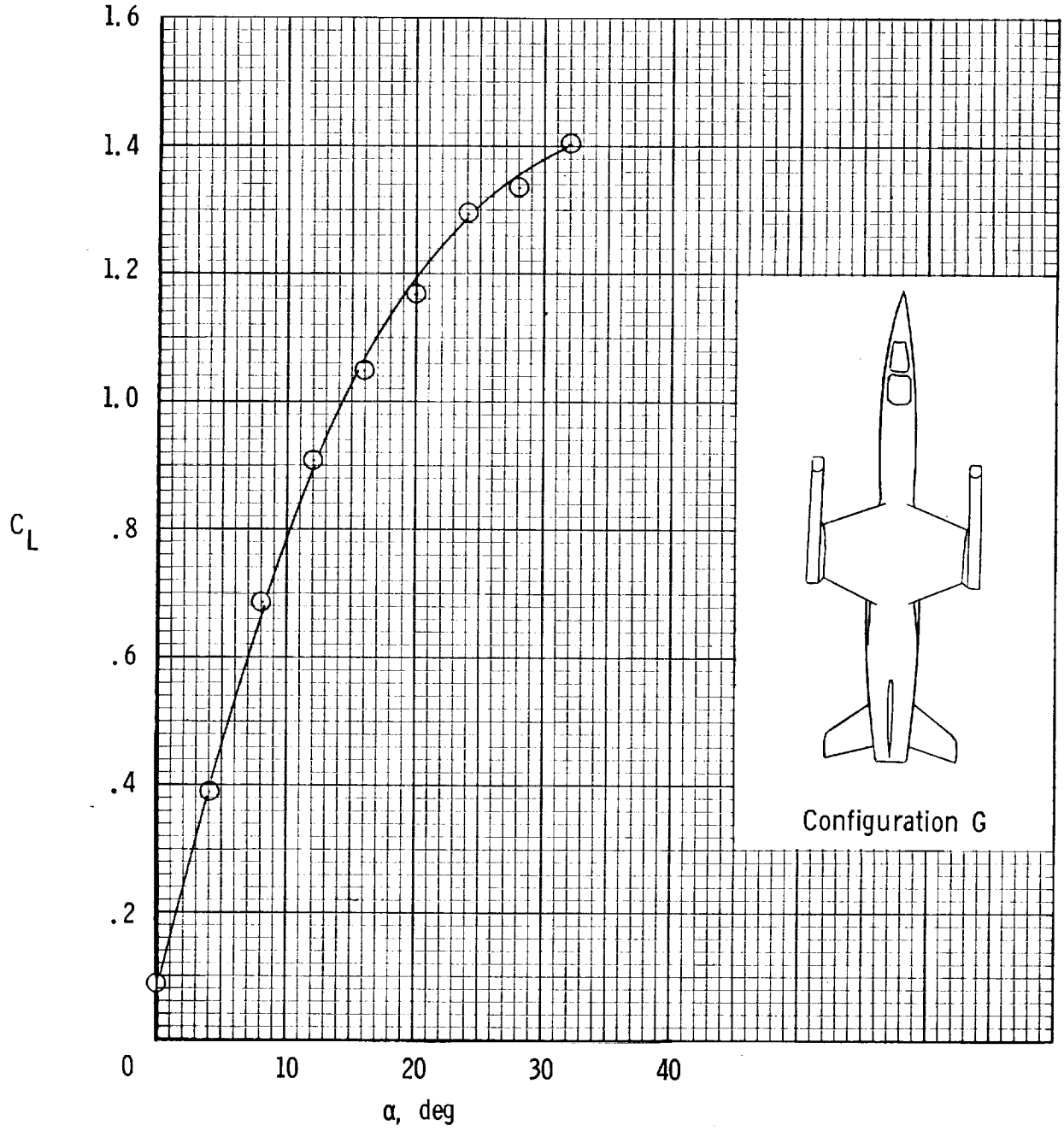

(a) Longitudinal characteristics.

Figure 12.- Longitudinal and lateral characteristics of configuration G (ref. 8).

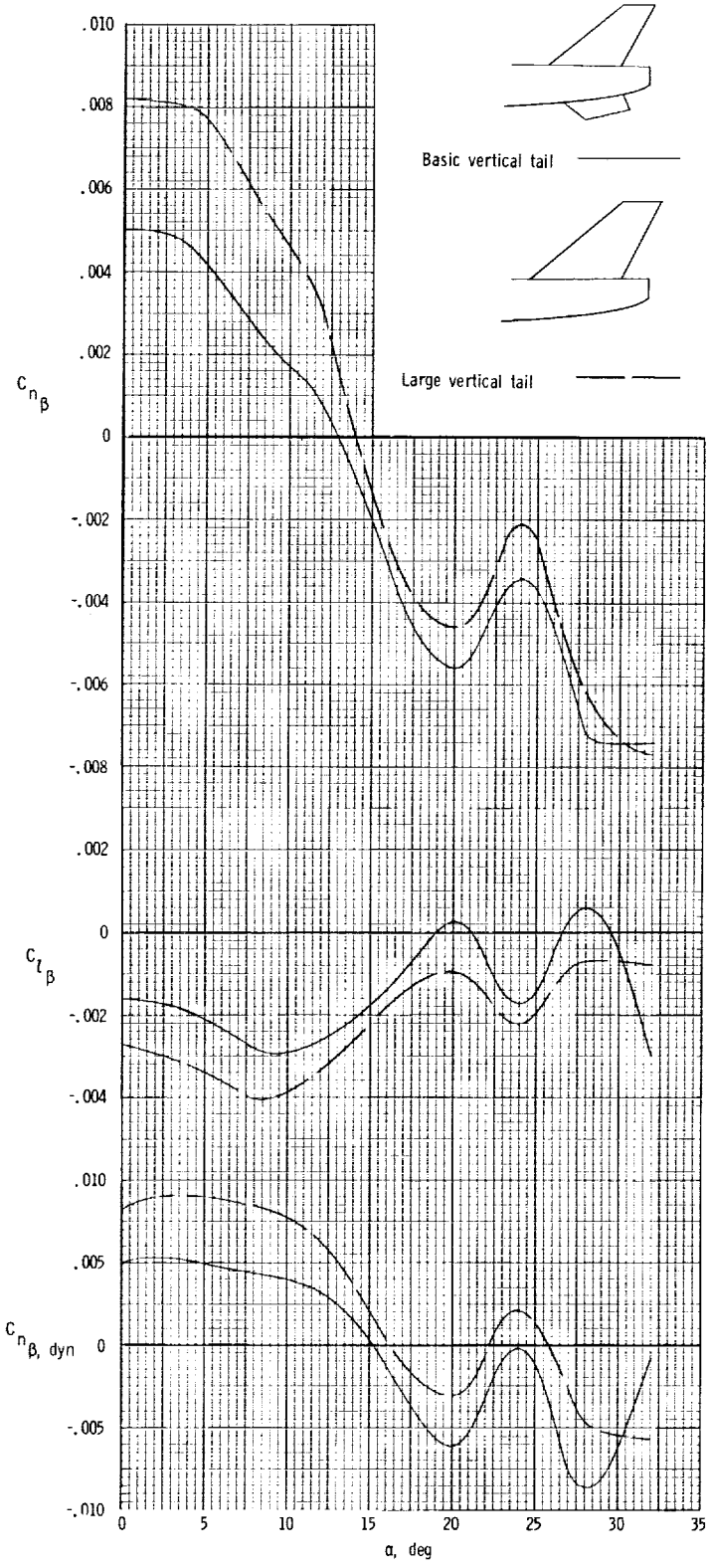

(b) Lateral characteristics. $\beta = \pm 5^{O}$.

Figure 12.- Concluded.

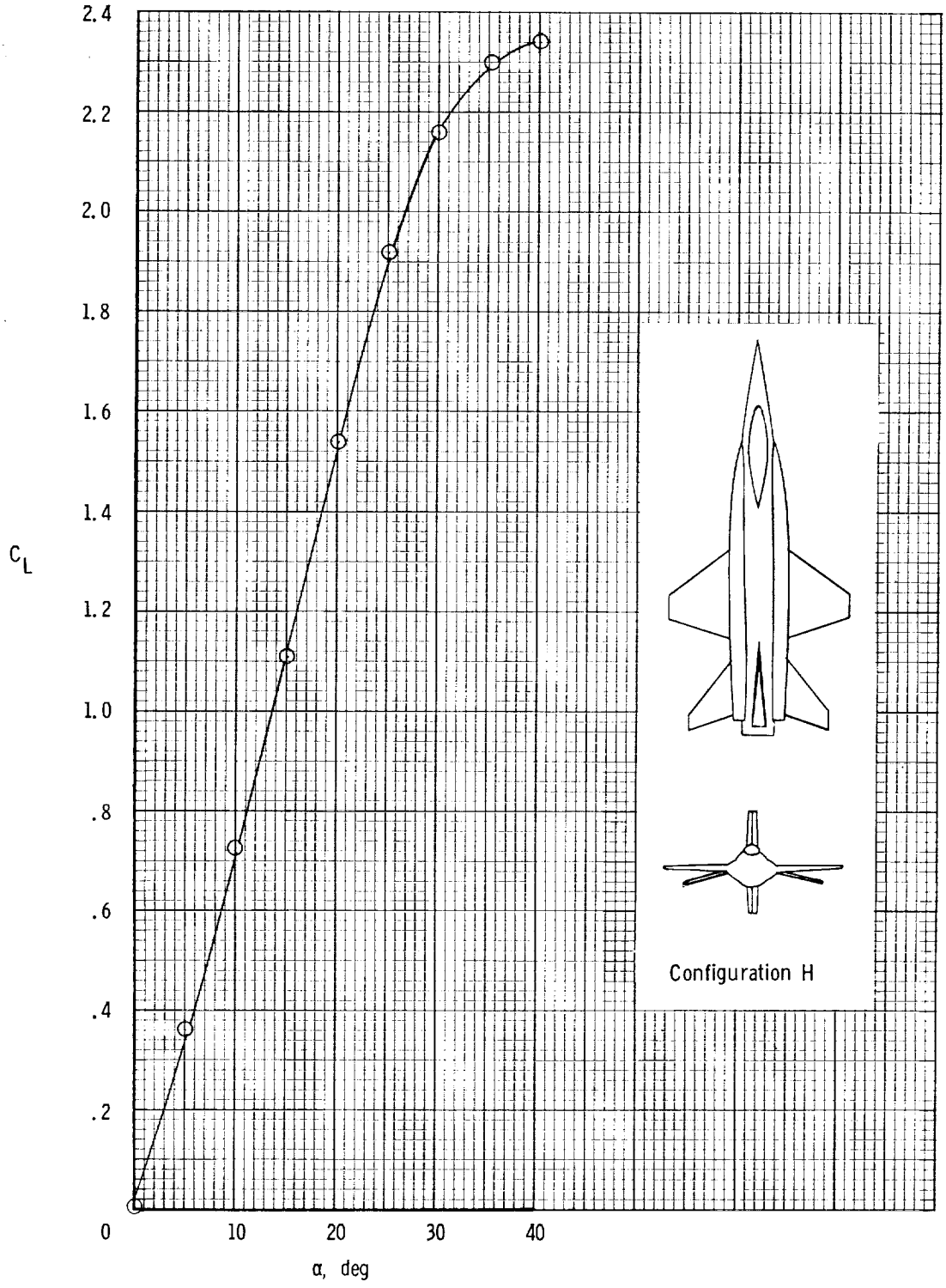

(a) Longitudinal characteristics.

Figure 13.- Longitudinal and lateral characteristics of configuration H (ref. 10).

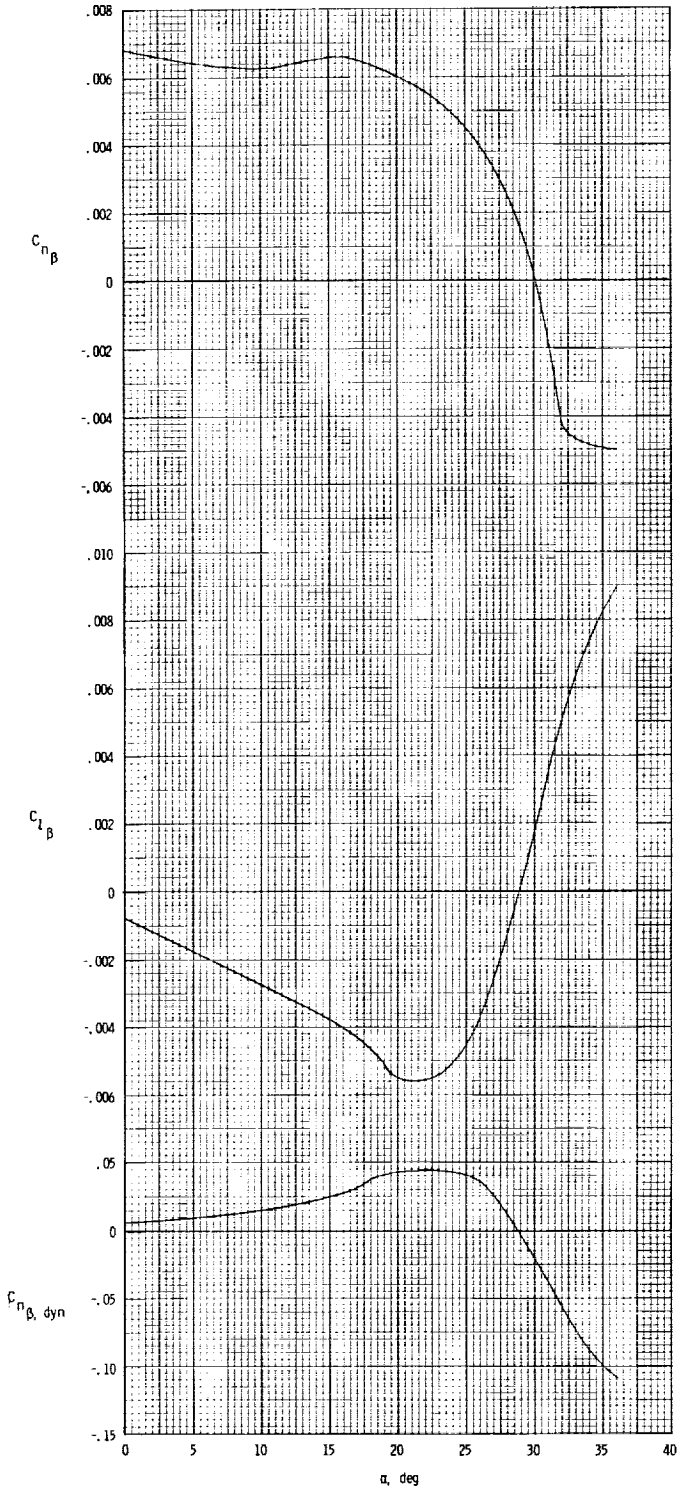

(b) Lateral characteristics. $\beta = \pm 5^{O}$.

Figure 13.- Concluded.

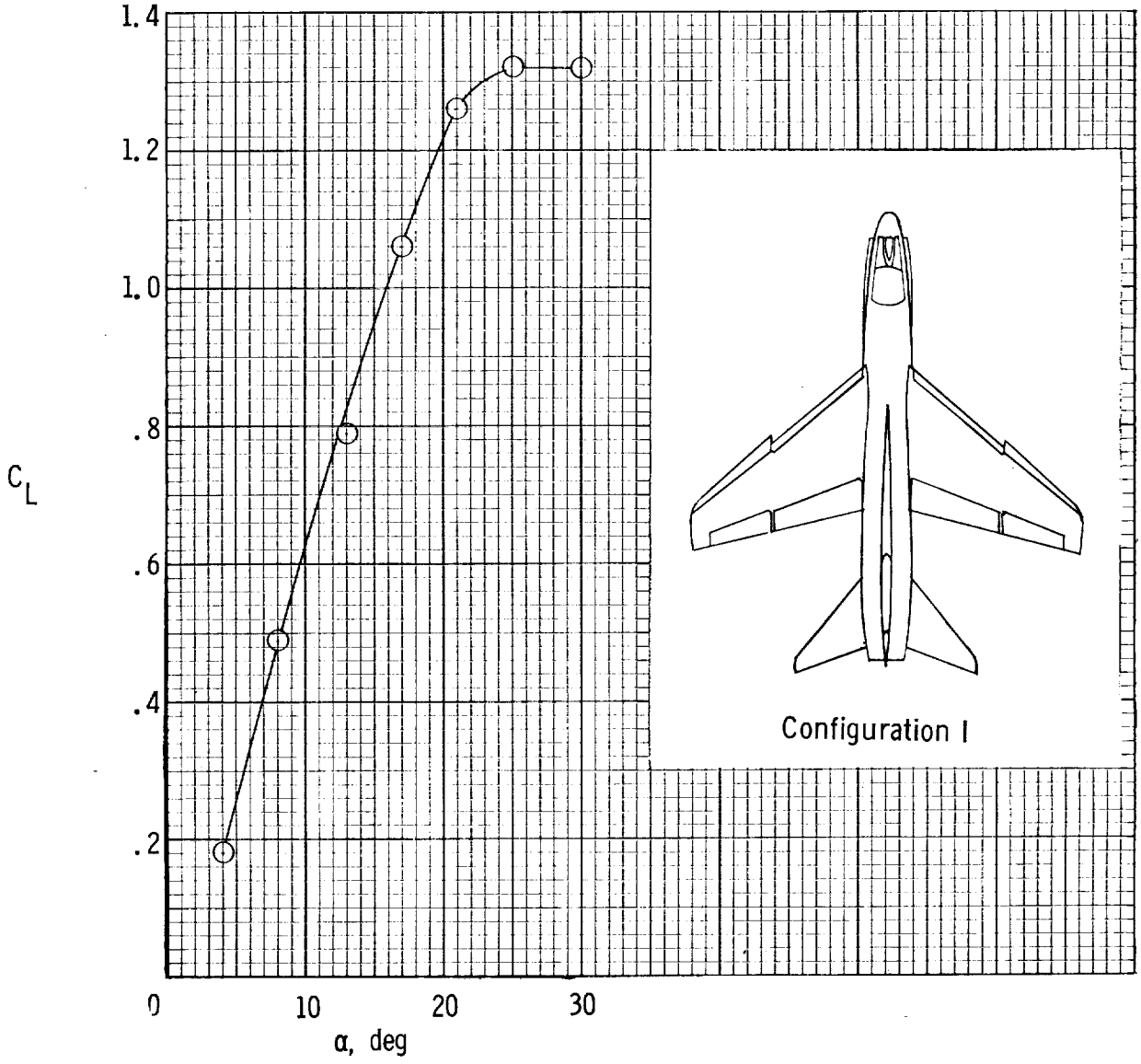

(a) Longitudinal characteristics.

Figure 14.- Longitudinal and lateral characteristics of configuration I (ref. 11 and unpublished data).

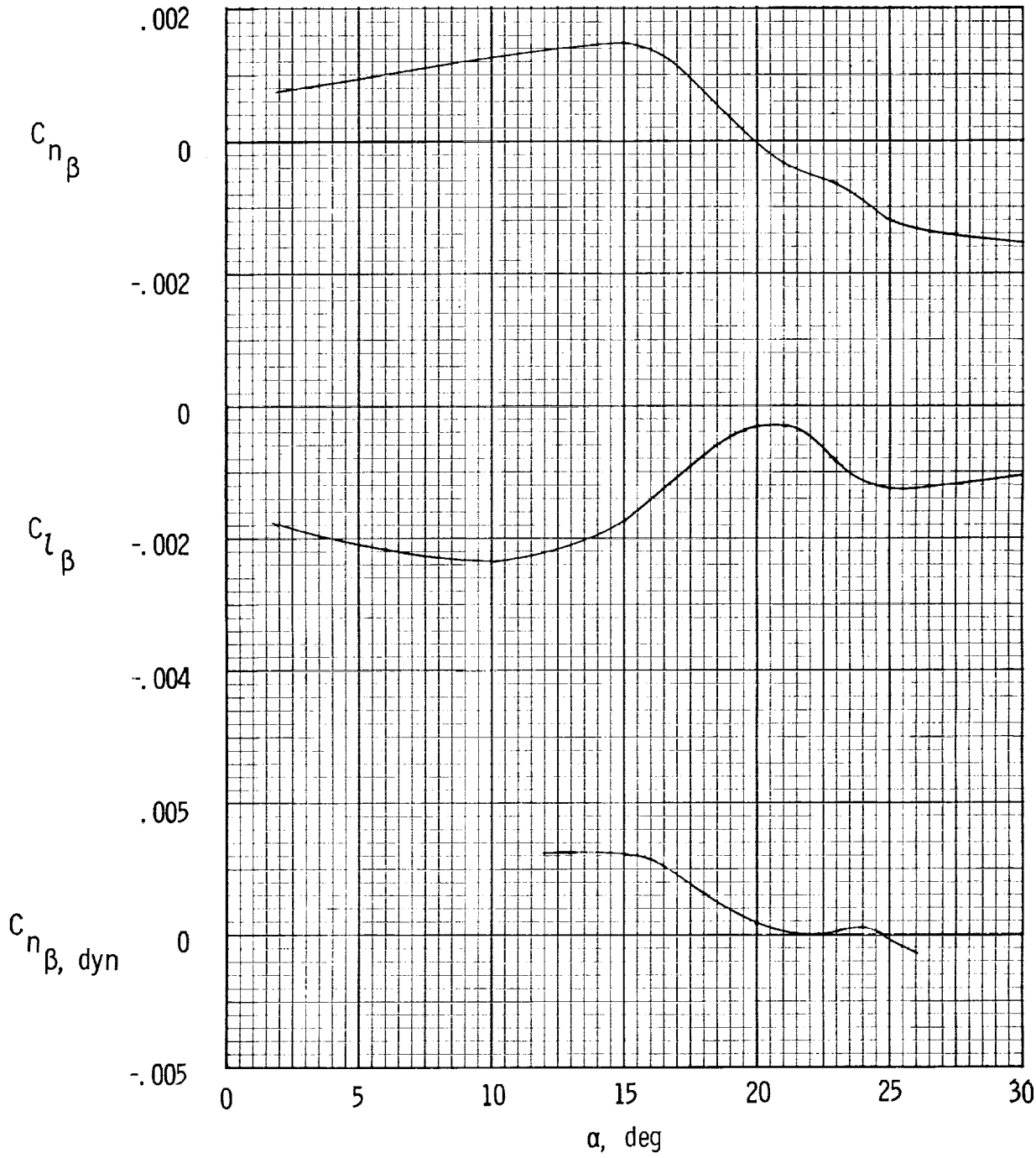

(b) Lateral characteristics.

Figure 14.- Concluded.

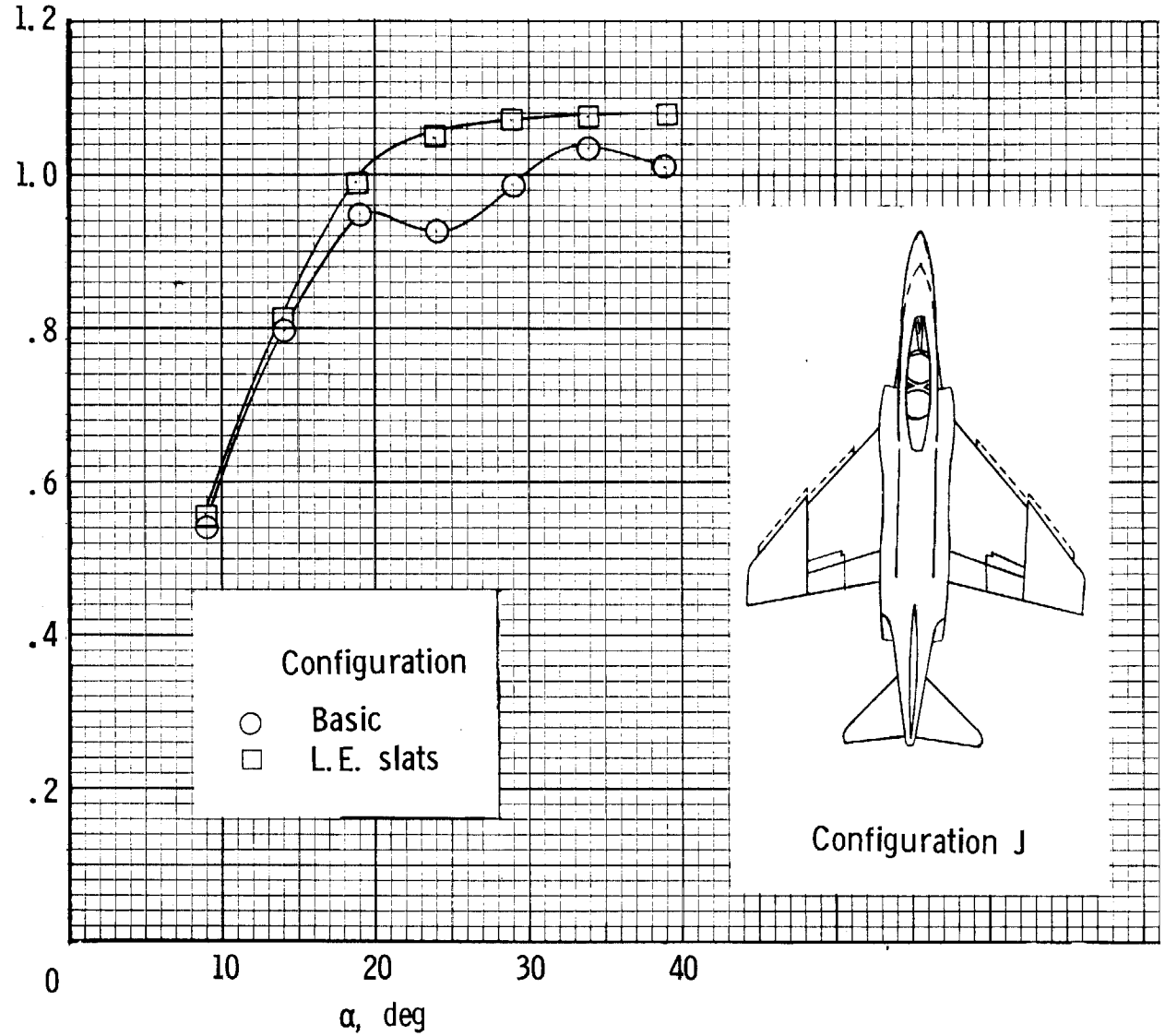

(a) Longitudinal characteristics.

Figure 15.- Longitudinal characteristics of configuration J (refs. 2 and 6).

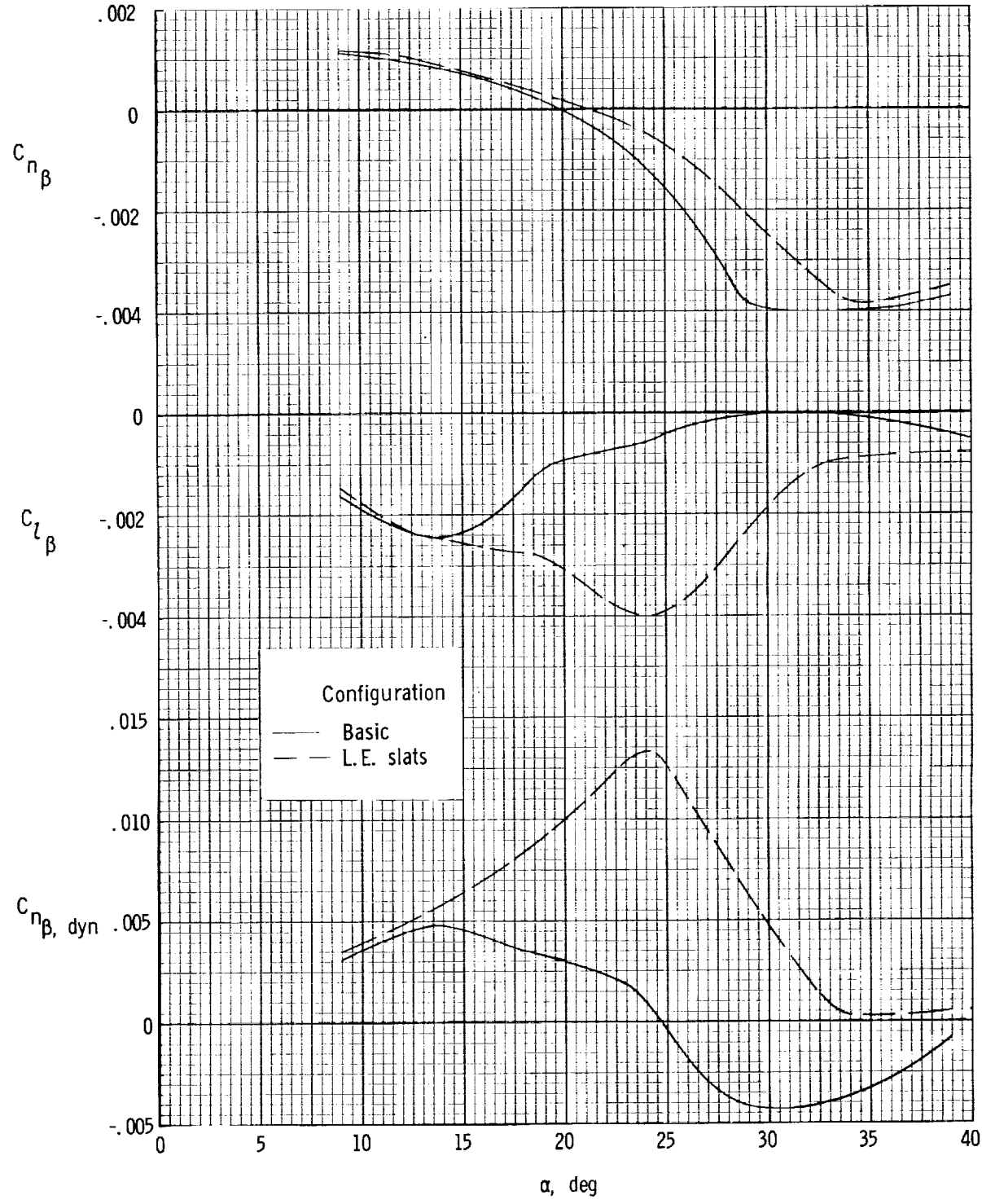

(b) Lateral characteristics. Long nose. $\beta = \pm 5^{o}$.

Figure 15.- Continued.

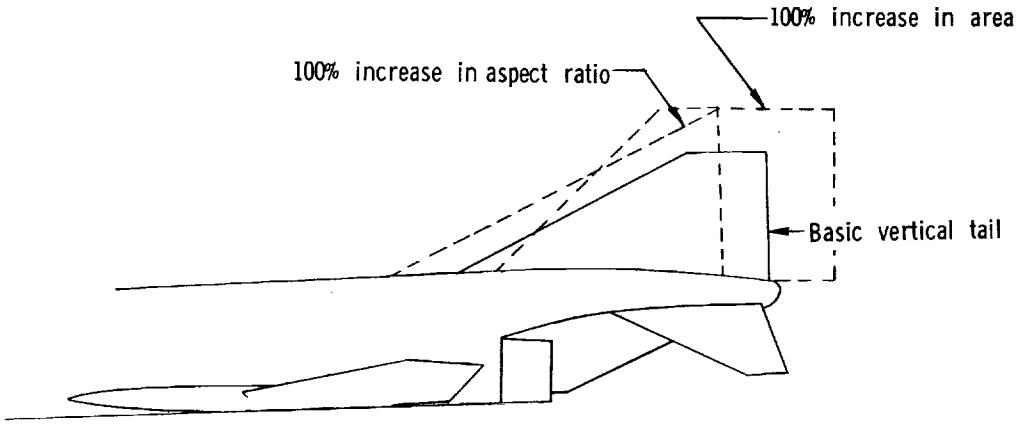

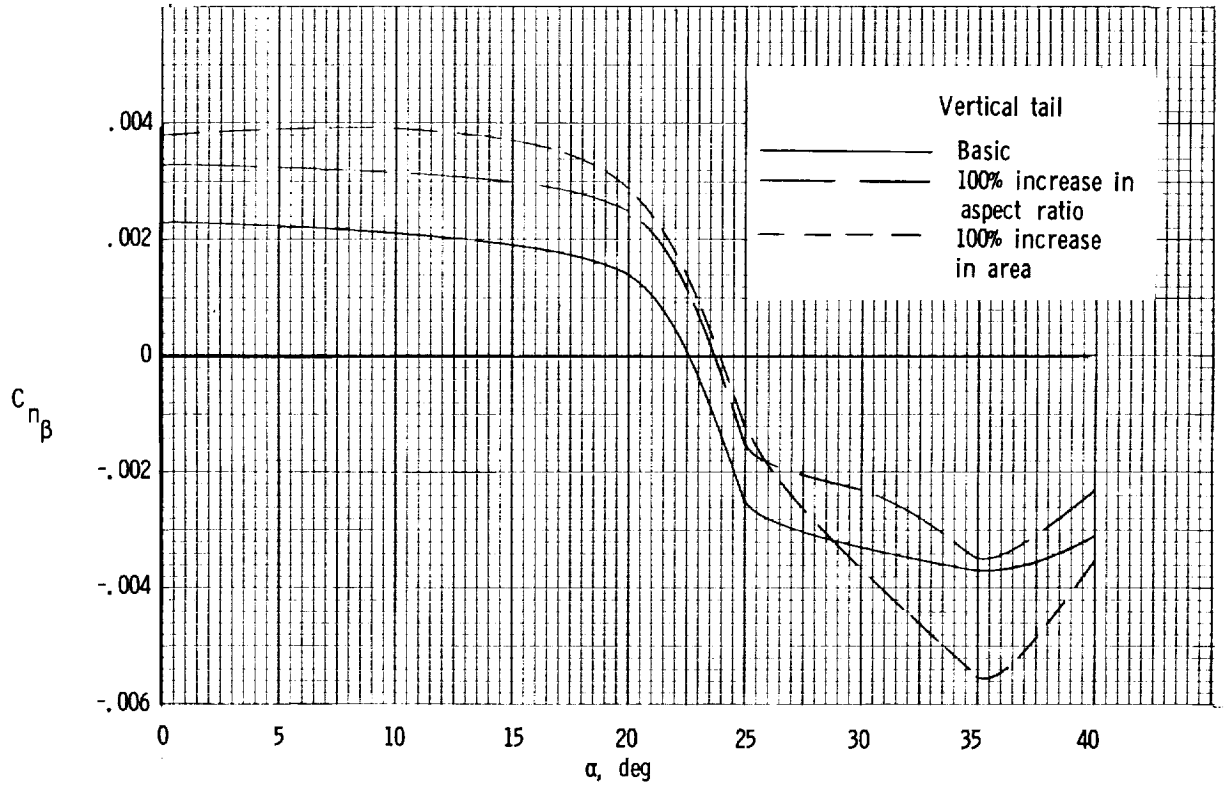

(c) Variation of C_{n_β} with vertical-tail size. Short nose. $\beta = \pm 5^{o}$.

Figure 15.- Concluded.

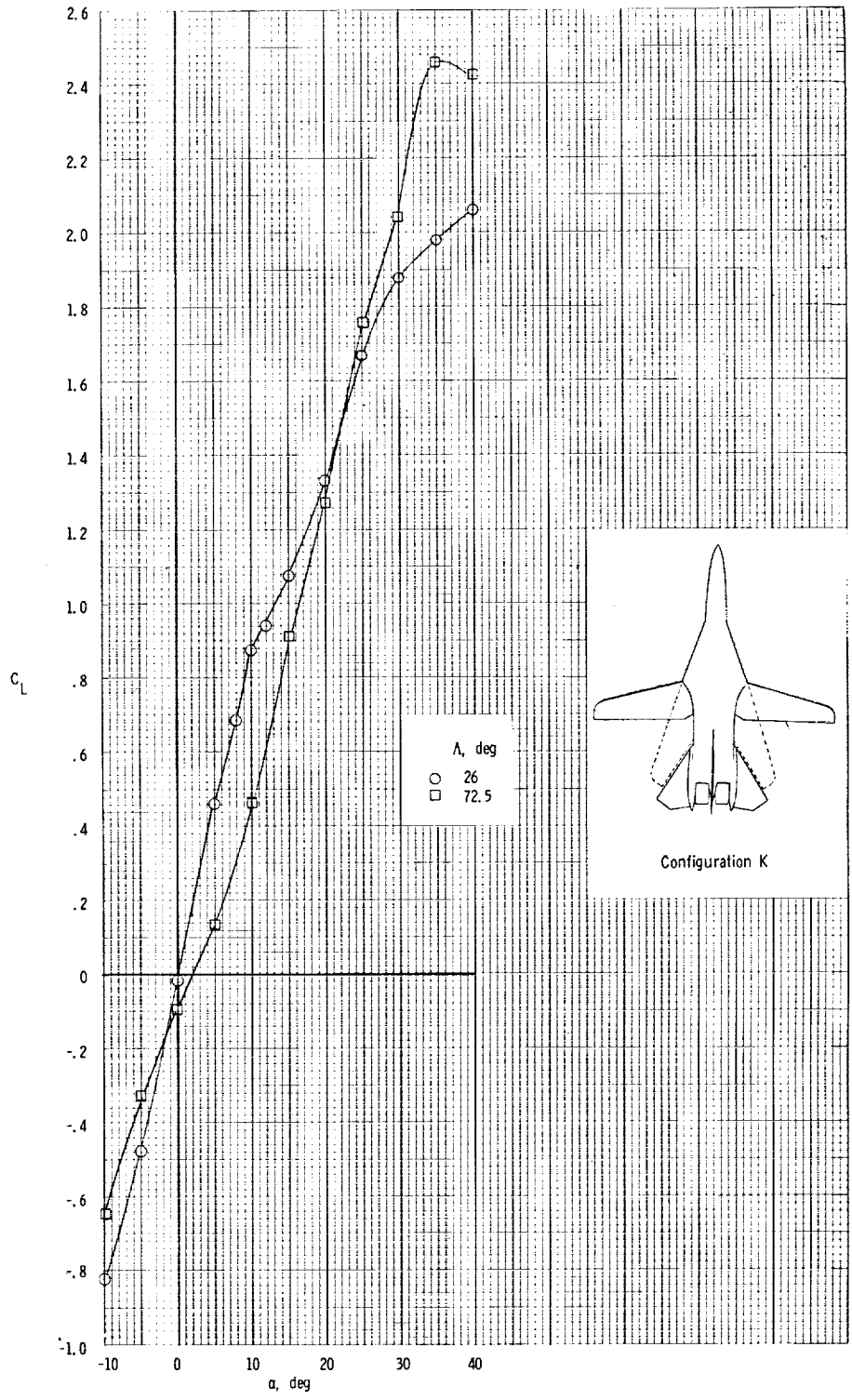

(a) Longitudinal characteristics.

Figure 16.- Longitudinal and lateral characteristics of configuration K (unpublished data).

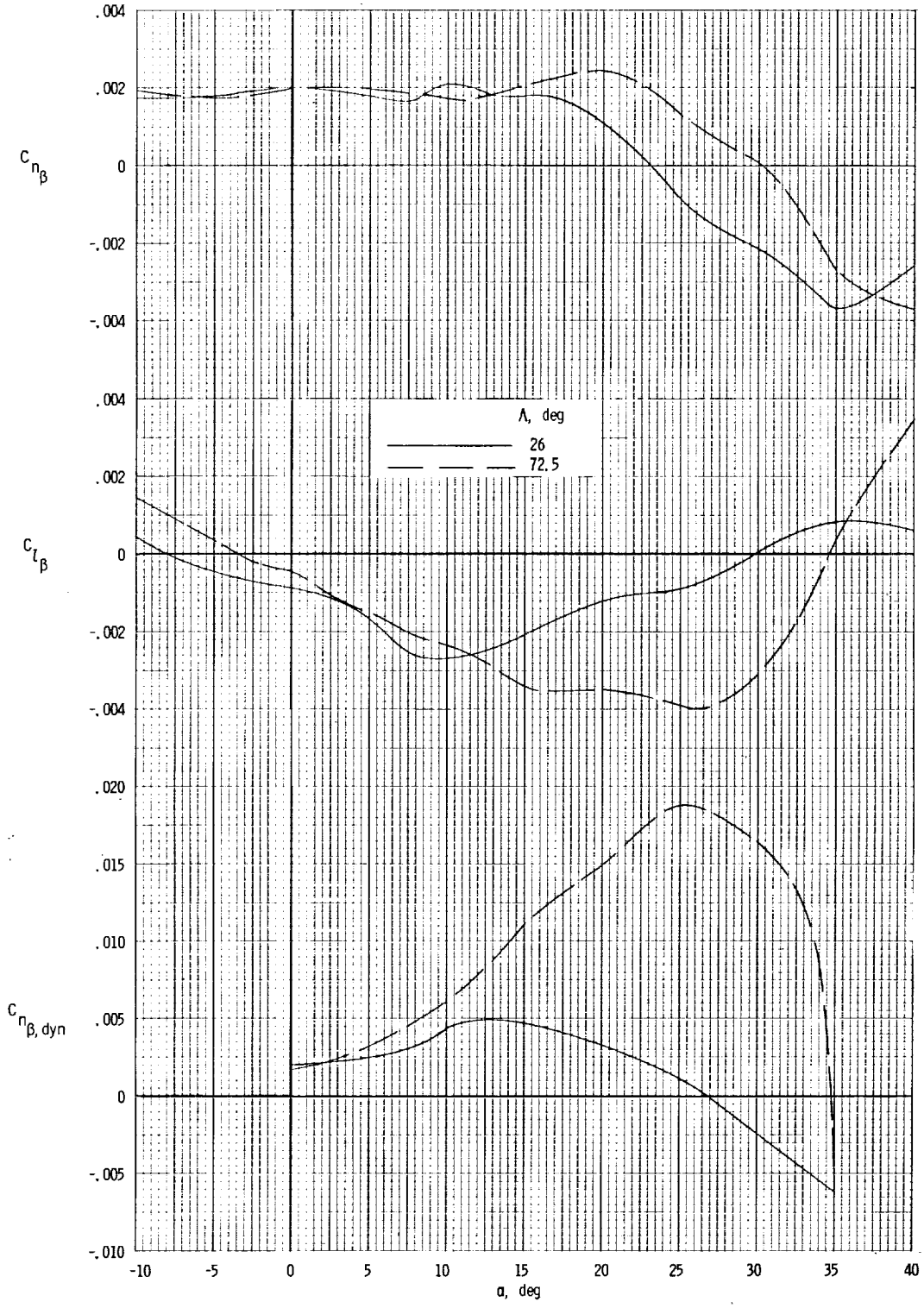

(b) Lateral characteristics. $\beta = \pm 5^{o}$.

Figure 16.- Concluded.

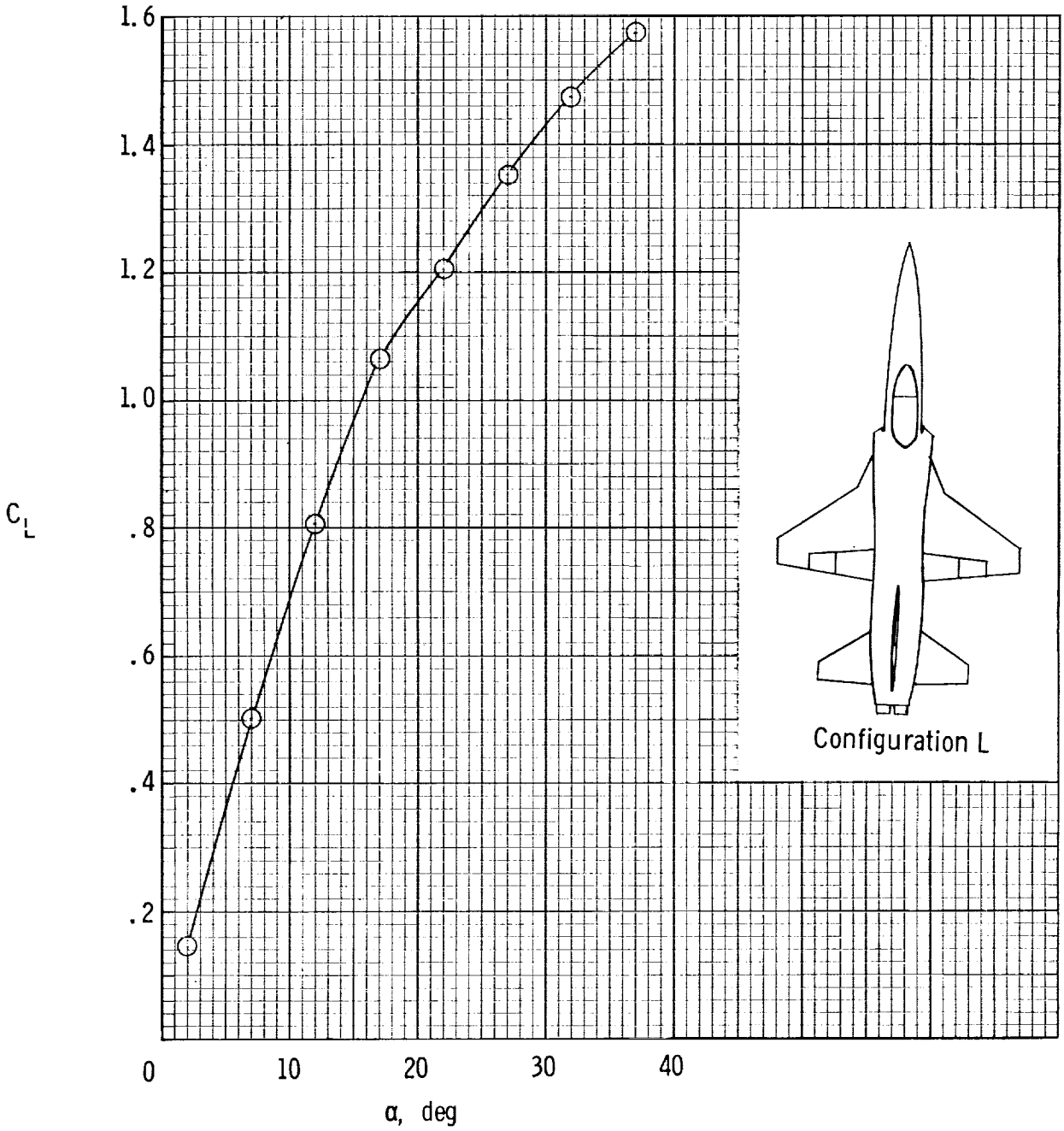

(a) Longitudinal characteristics.

Figure 17.- Longitudinal and lateral characteristics of configuration L (unpublished data).

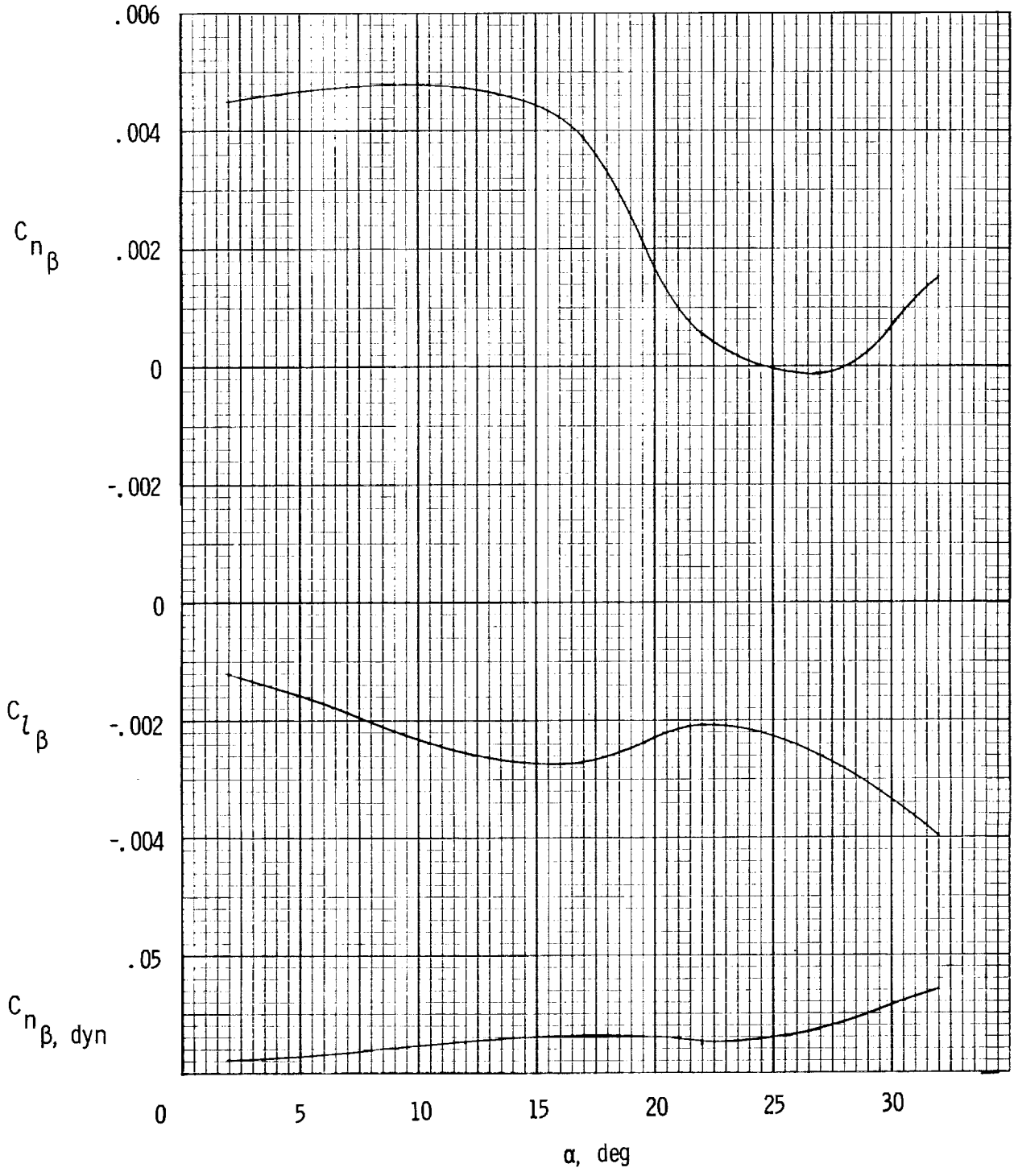

(b) Lateral characteristics. $\beta = \pm 5^{o}$.

Figure 17.- Concluded.

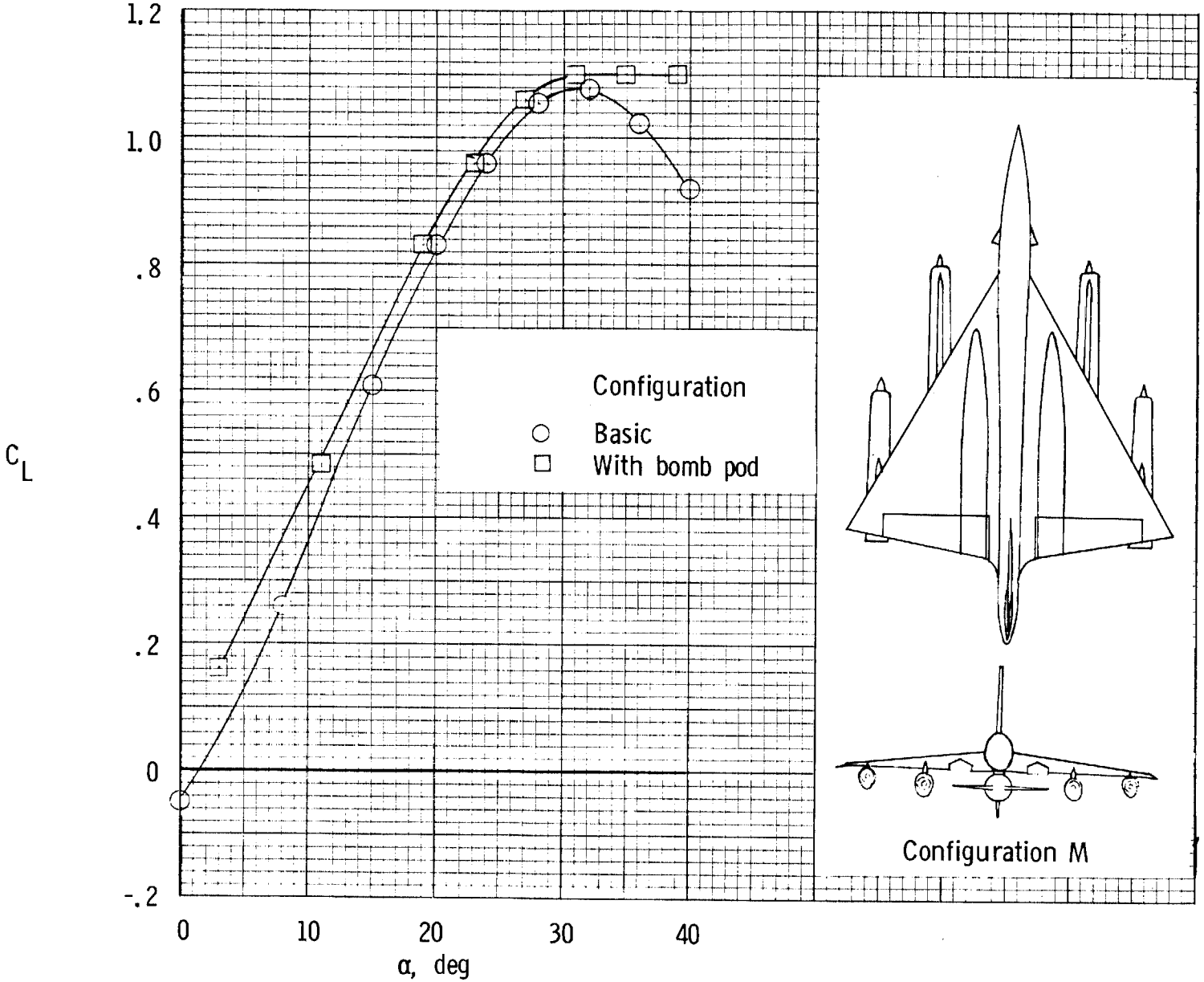

(a) Longitudinal characteristics.

Figure 18.- Longitudinal and lateral characteristics of configuration M (ref. 12).

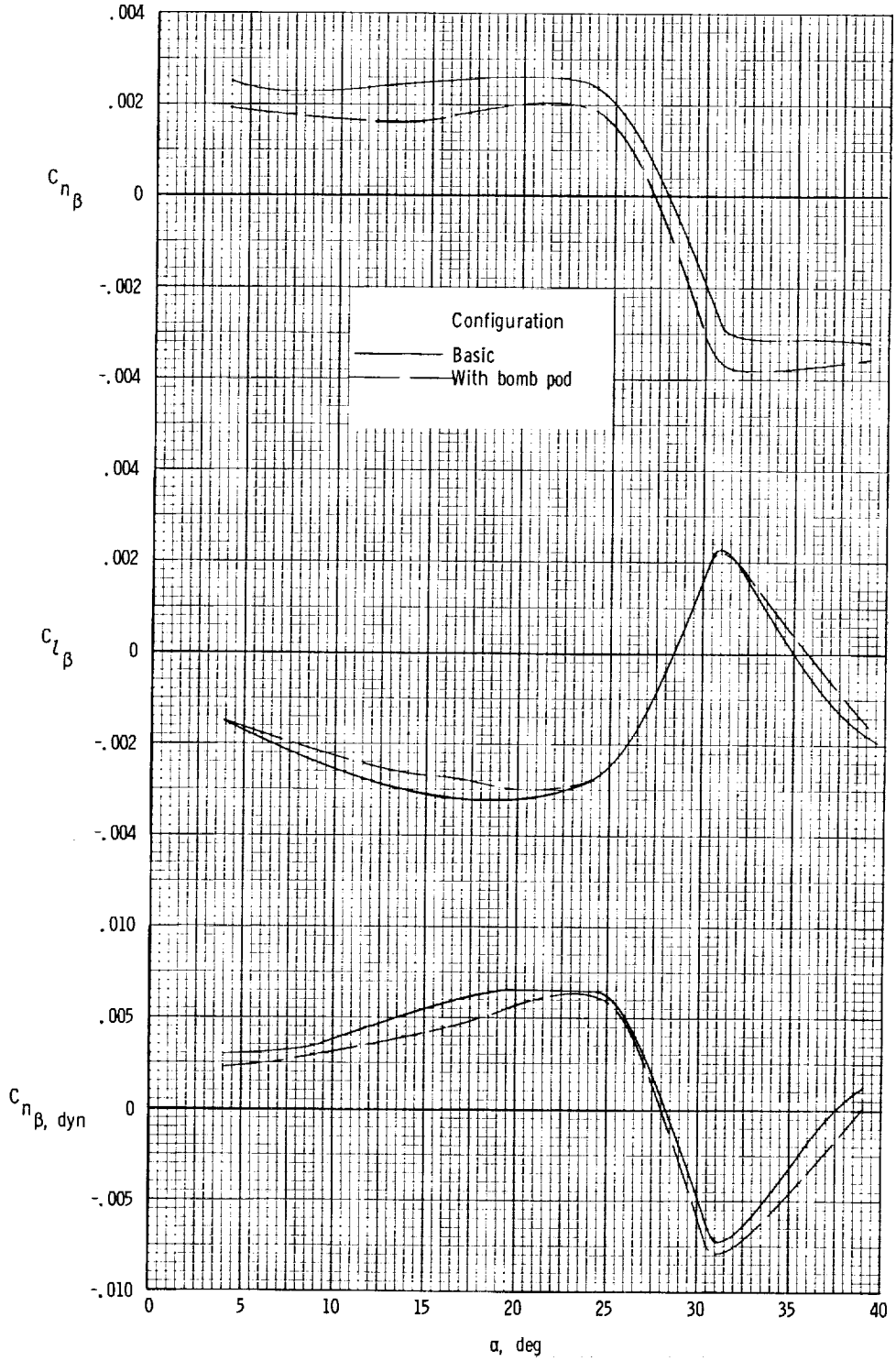

(b) Lateral characteristics. $\beta = \pm 5^{o}$.

Figure 18.- Concluded.

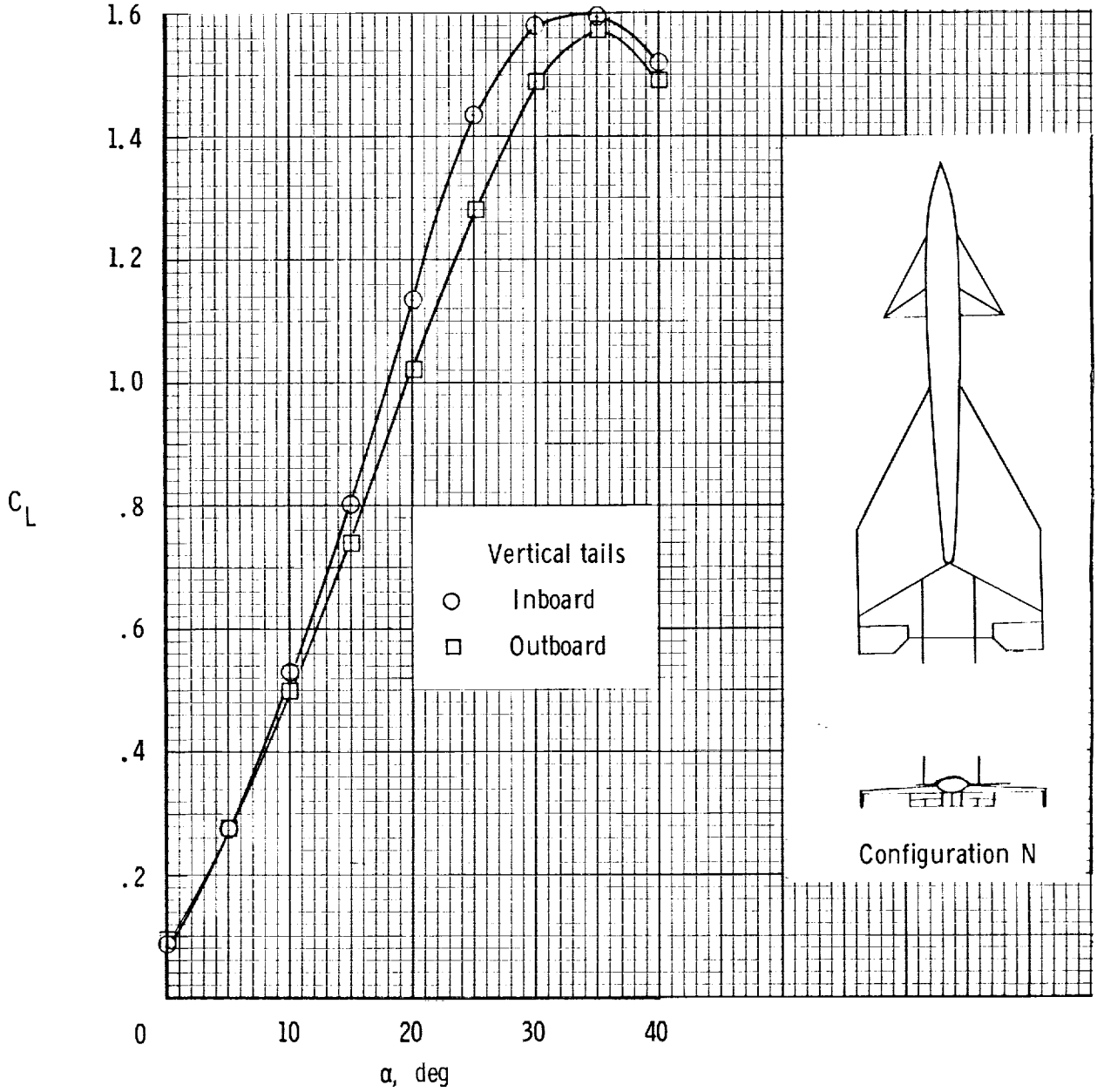

(a) Longitudinal characteristics.

Figure 19.- Longitudinal and lateral characteristics of configuration N (unpublished data).

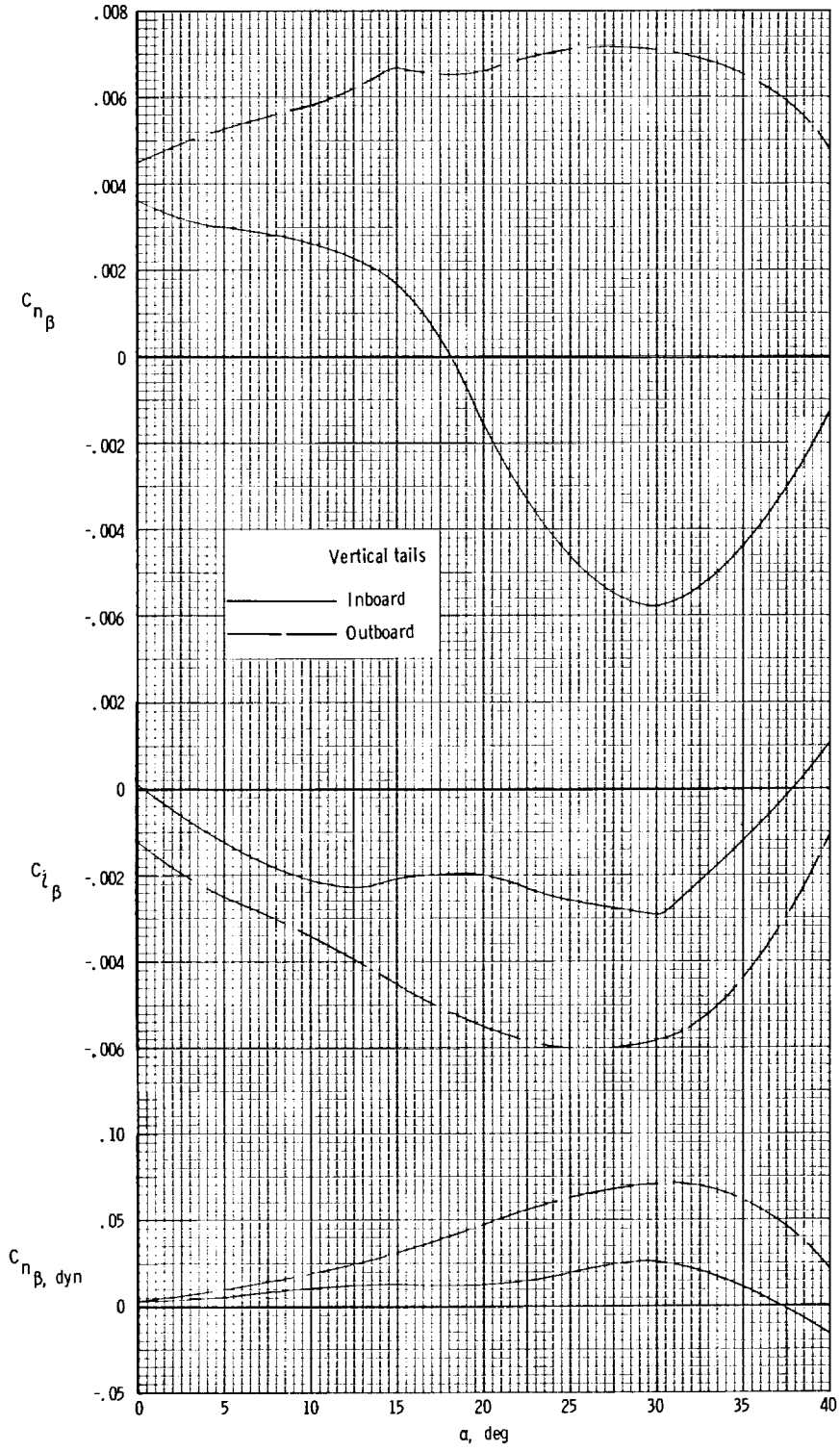

(b) Lateral characteristics. $\beta = \pm 5^{o}$.

Figure 19.- Concluded.

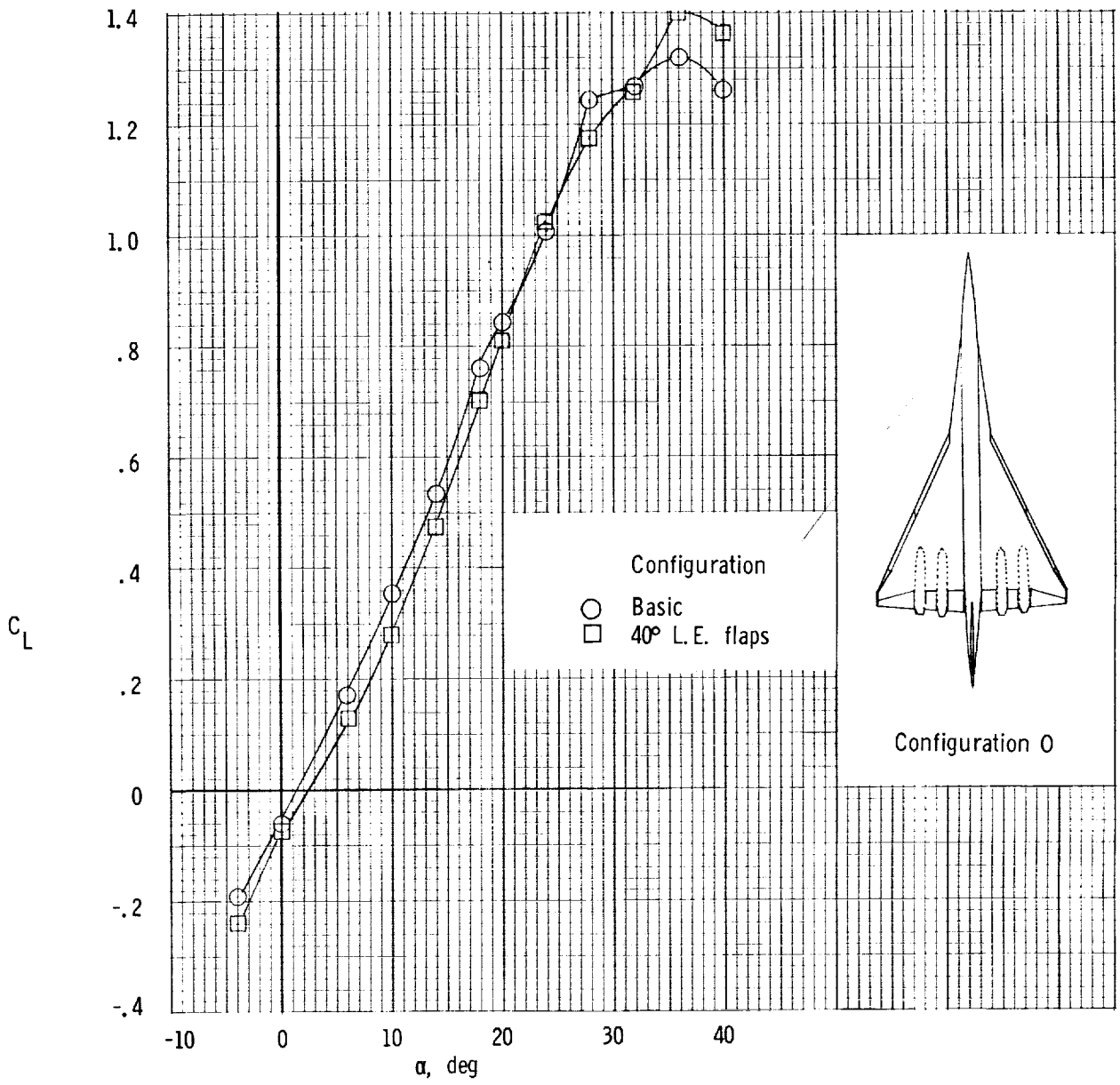

(a) Longitudinal characteristics.

Figure 20.- Longitudinal and lateral characteristics of configuration O (ref. 13).

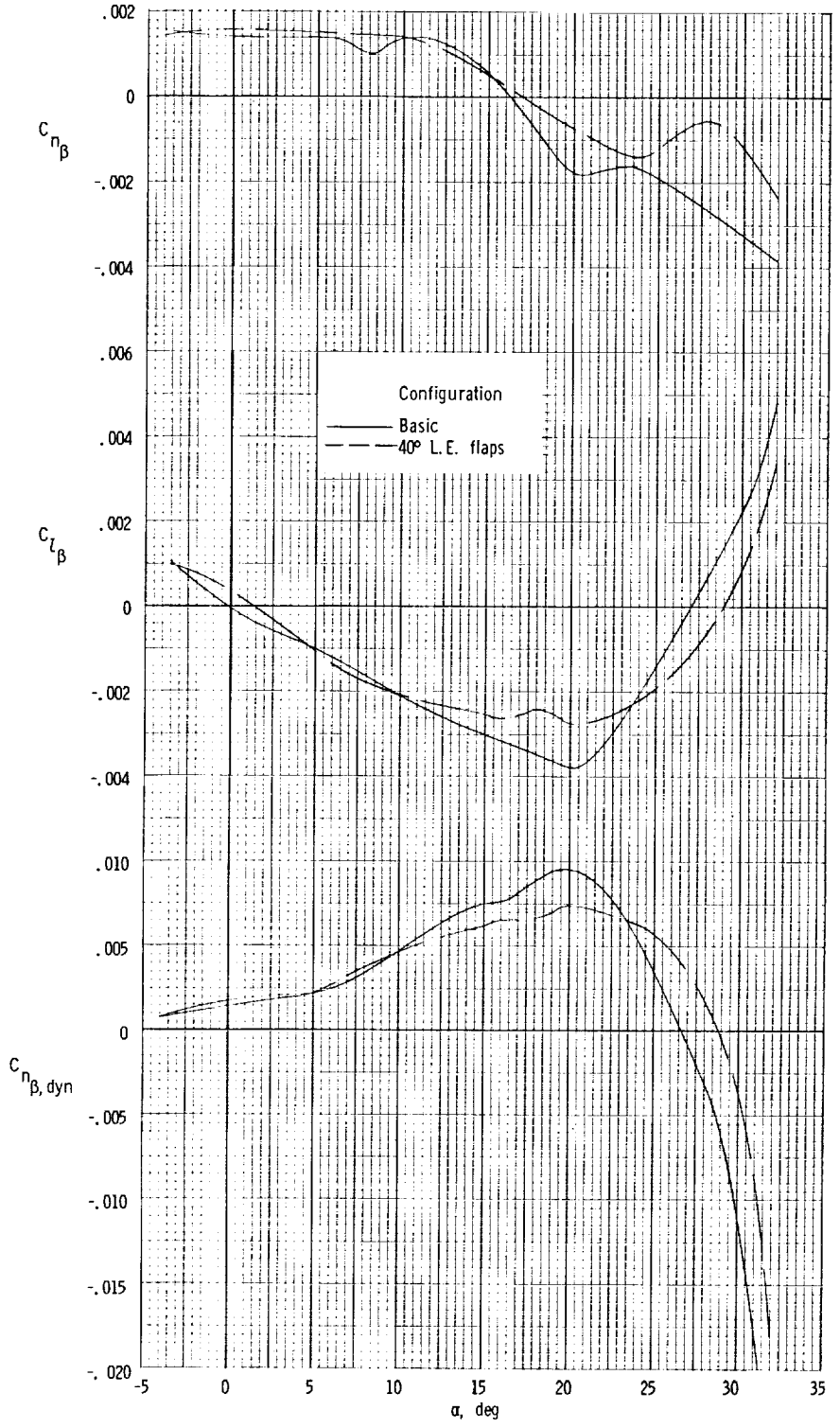

(b) Lateral characteristics. $\beta = \pm 5^{O}$.

Figure 20.- Concluded.

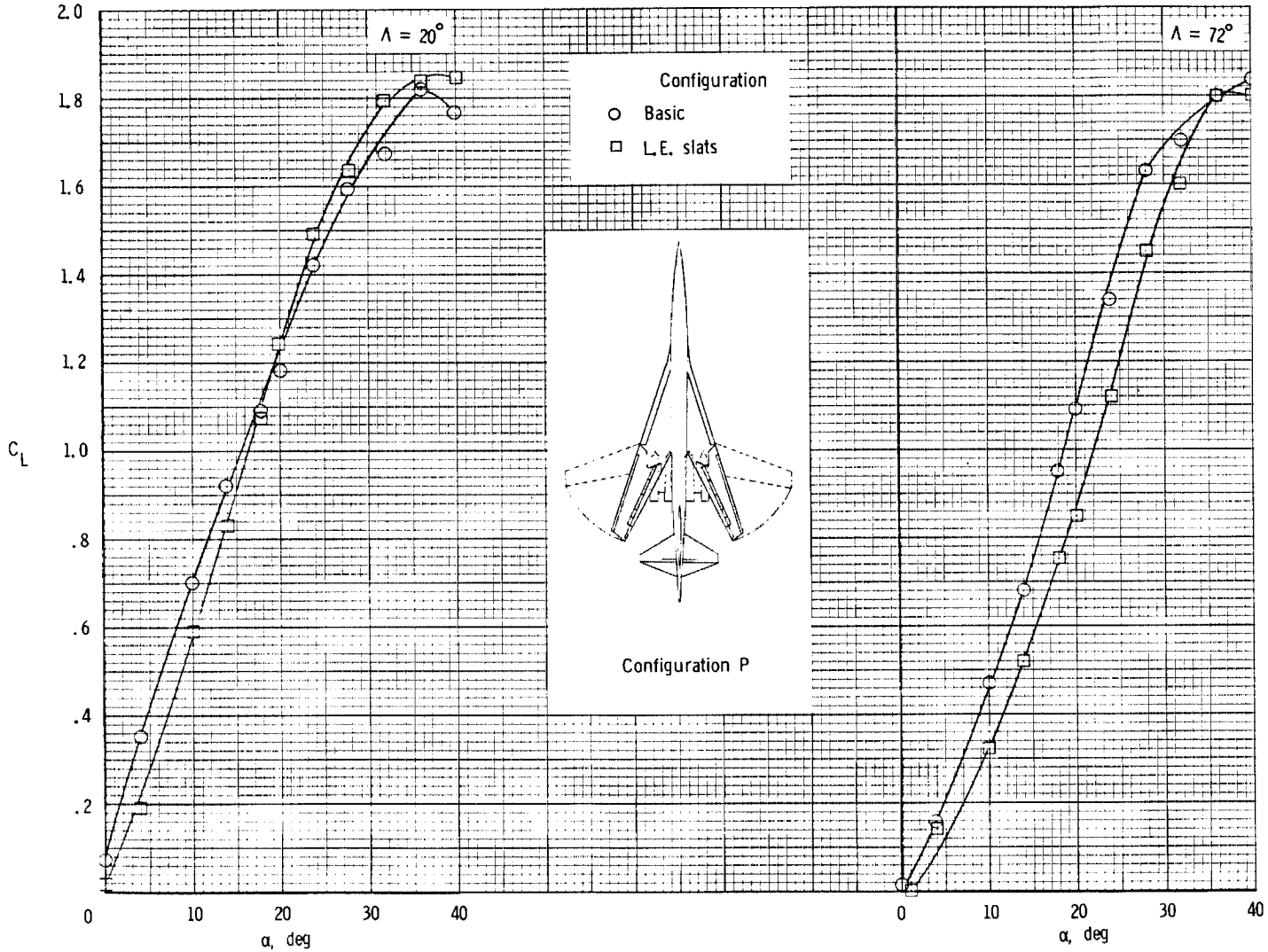

(a) Longitudinal characteristics.

Figure 21.- Longitudinal and lateral characteristics of configuration P (ref. 9).

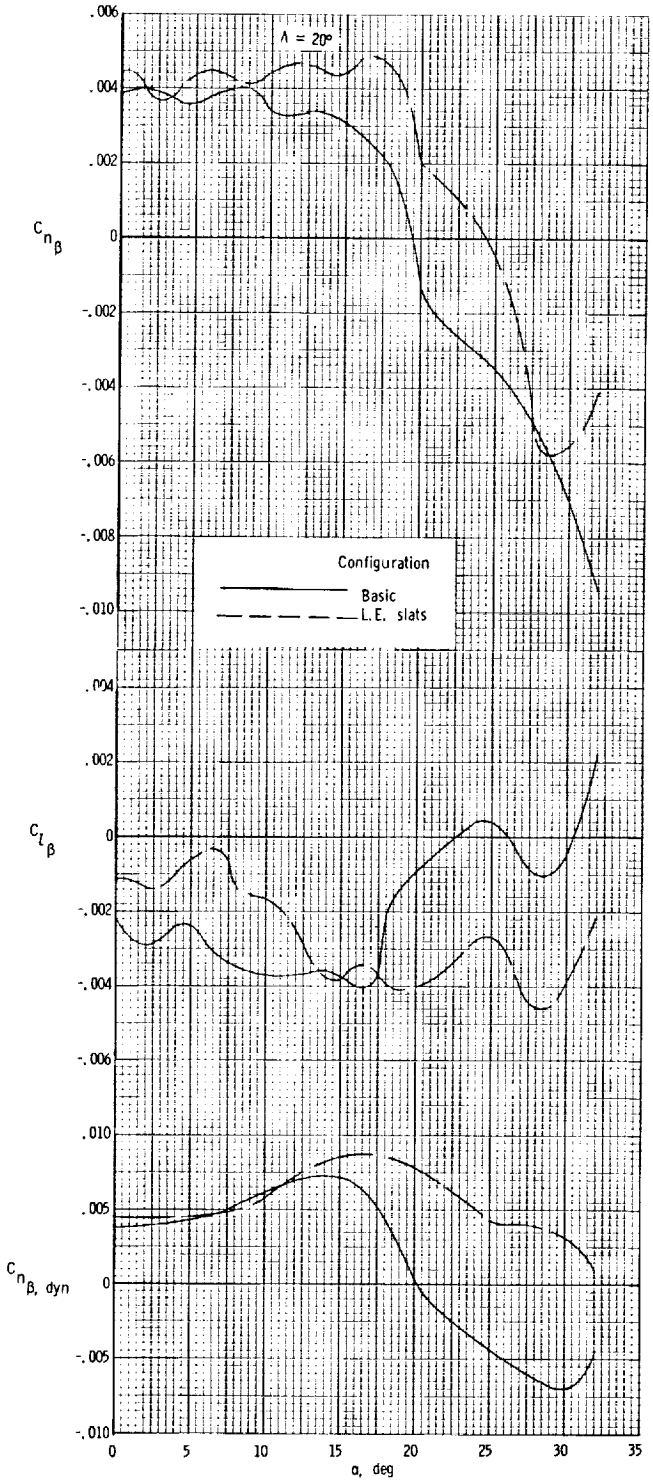

(b) Lateral characteristics. $\beta = \pm 5^{O}$.

Figure 21.- Continued.

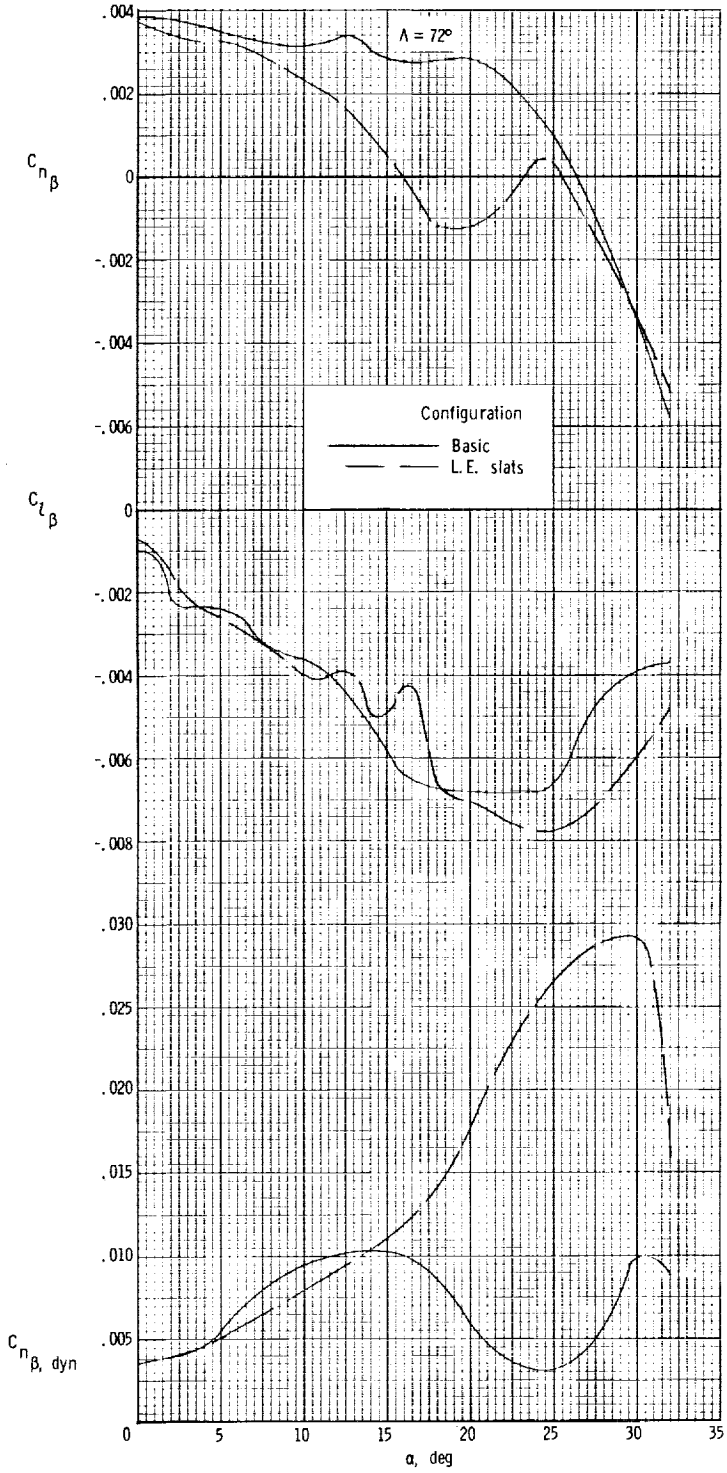

(b) Concluded.

Figure 21.- Concluded.

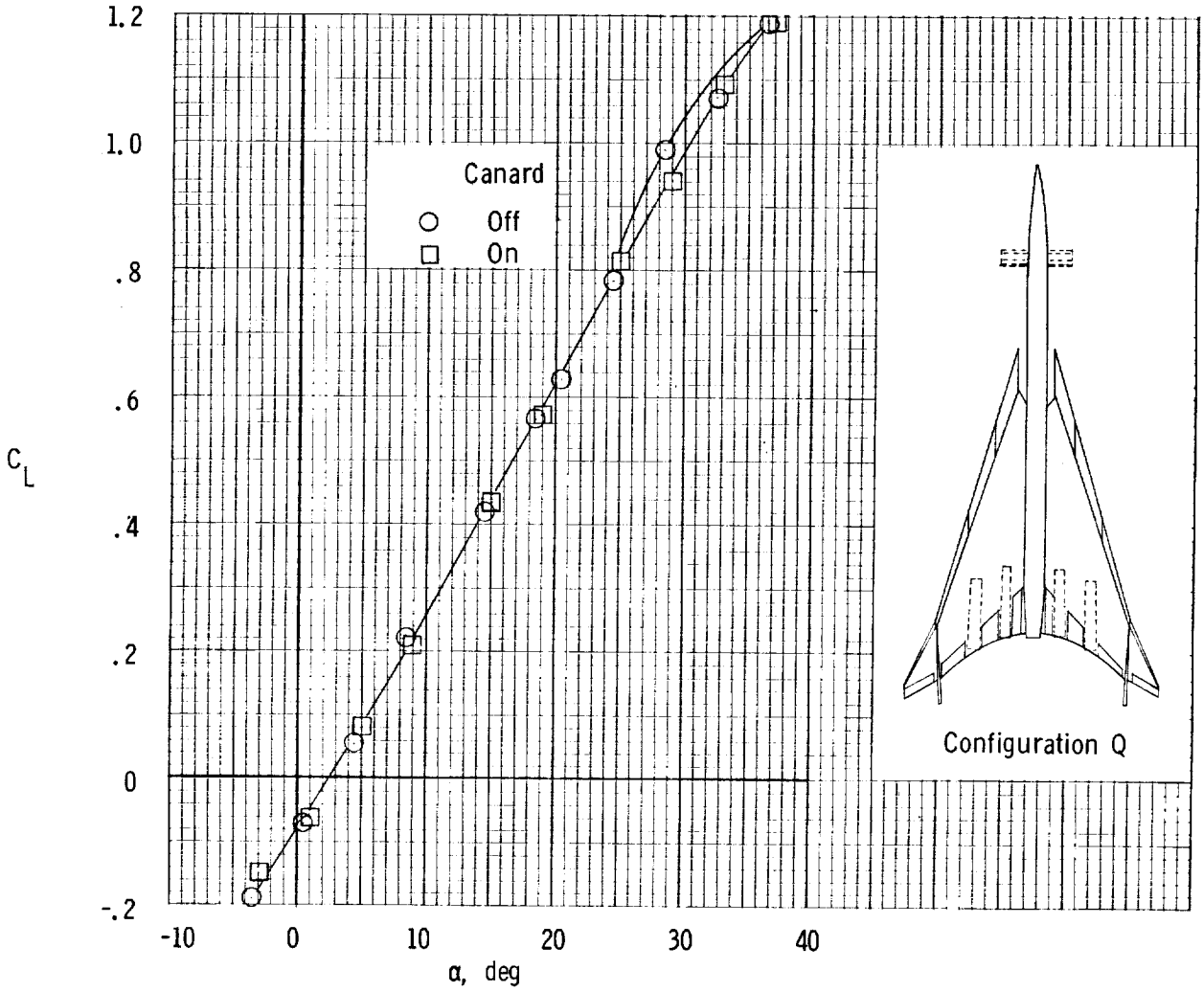

(a) Longitudinal characteristics.

Figure 22.- Longitudinal and lateral characteristics of configuration Q (ref. 14).

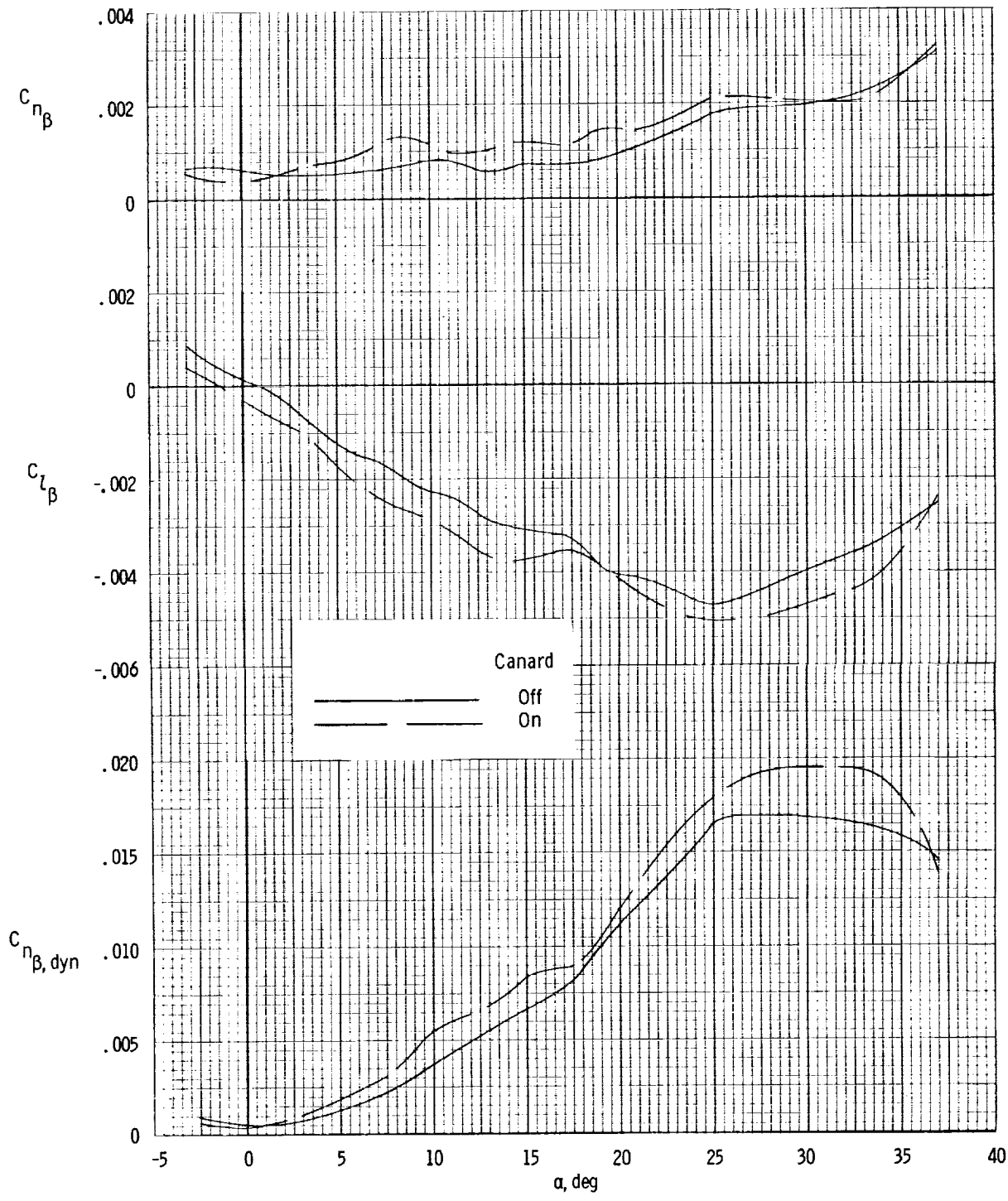

(b) Lateral characteristics. $\beta = \pm 5^{o}$.

Figure 22.- Concluded.

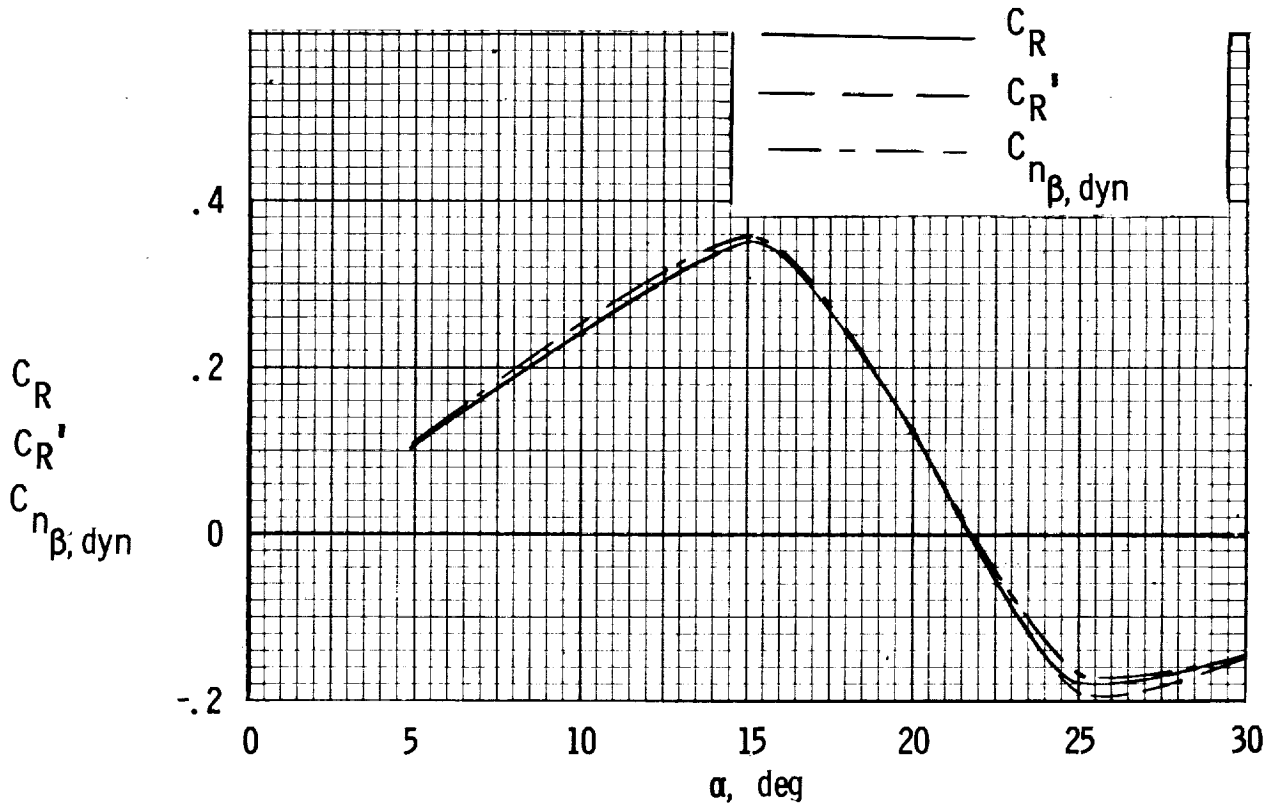

(a) Configuration J. Short nose.

Figure 23.- Comparison of C_R with C_R' and $C_{n_{\beta,dyn}}$ for two configurations.

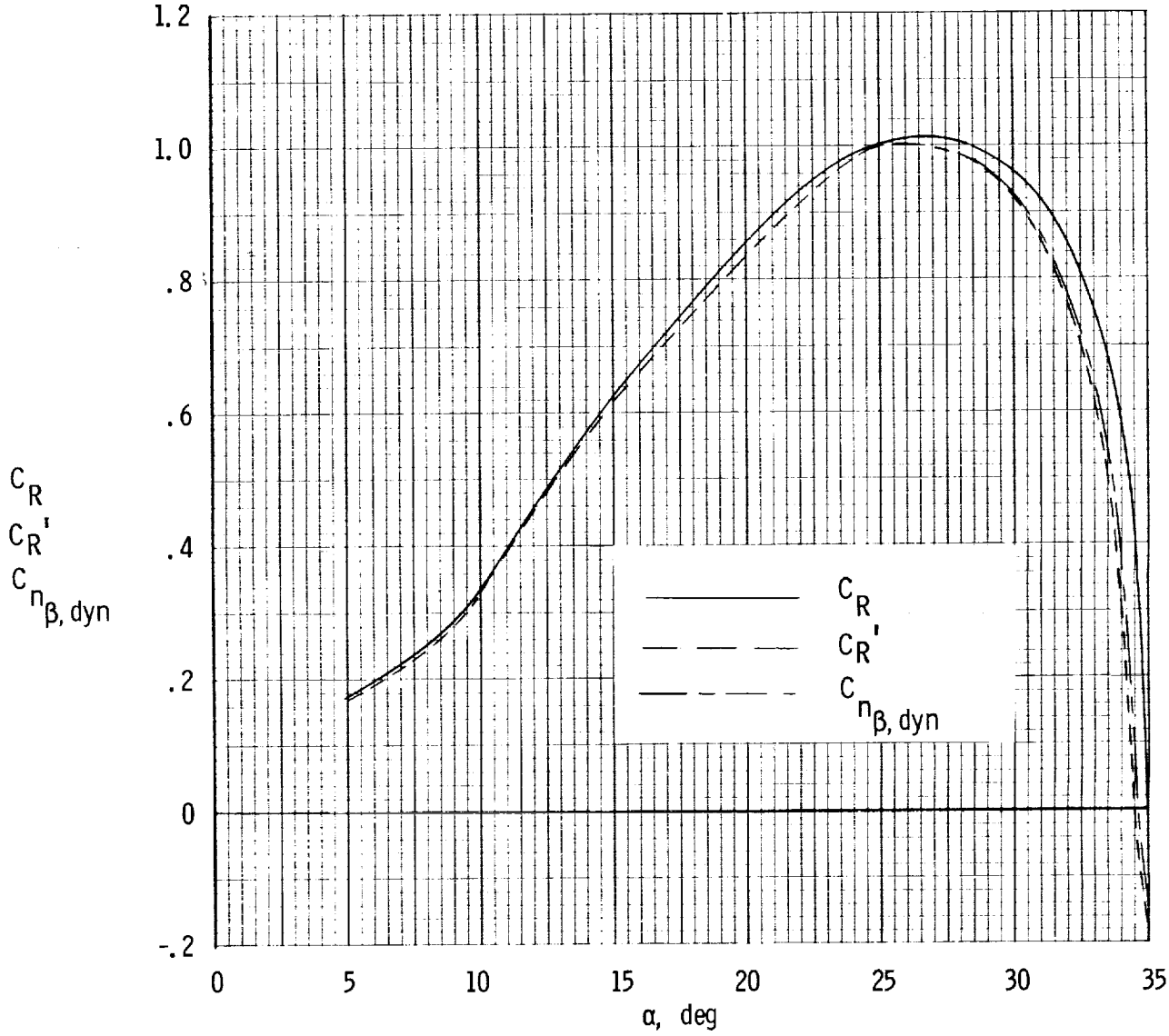

(b) Configuration K. $\Lambda = 72.5^{\circ}$.

Figure 23.- Concluded.

NASA-Langley, 1972 — 2 L-8489